Soft Condensed Matter

Lectures 12-22

Ulrich F. Keyser
ufk20@cam.ac.uk

Lent and Easter Terms 2023
Version: January 9, 2023

Foreword

These lecture notes summarise some of the material from lectures 12-22 on *Soft Condensed Matter* and adds some background reading. I am grateful to Tuomas Knowles for many useful discussions, and to Pietro Cicuta and Eugene Terentjev for providing an abundance of material that inspired the choice of topics and provided the basis of these notes. I thank Alice Thorneywork, Mustafa Caglar, Jeffrey Mc Hugh, Harry McMullan, and many undergraduate students for proof reading of these notes and helpful suggestions.

In case you find mistakes please send an email to ufk20 (at) cam.ac.uk.

Contents

Chapter 7

Self-assembly: Part II

7.1 Membranes

Lipid membranes are ubiquitous in biological systems. They act as a diffusion barrier for charged molecules and ions, provide scaffolding for membrane proteins and represent an important, structural, and even active component of most living systems. In this chapter we will discuss some of the properties of bilayers that are a direct consequence of the self-assembly of their main components - amphiphilic molecules. More specifically we will look at lipid bilayer shape and phase, curvature and membrane fluctuations. The chapter ends with a brief discussion on self assembly in biological systems beyond lipid membranes.

7.2 Lipid Bilayers

Lipid bilayers consist of double layer of amphiphilic molecules as shown in the previous chapter. In aqueous solutions the hydrophobic tails are forming an oil like film while the hydrophilic head-groups surround the tails and make the layers overall hydrophilic. In this chapter we will discuss the dynamic nature of lipid bilayers, a direct consequence of the numerous different phases and resulting geometries that the system can adopt. The different phases have a range of different mechanical characteristics and are usually reached by first order phase transitions. Biological cells tune the parameters of these thin membranes by tuning the exact composition and hence carefully control the phase transition temperature and state.

Self-assembled lipids structures can exist in different many different phases. Four examples with increasing water content are shown in Figure 7.1. The four phases are known as hexagonal (H), layered (L), cubic (Q) and as vesicle (V). The names are self explanatory. The most important phases for this course are L and V.

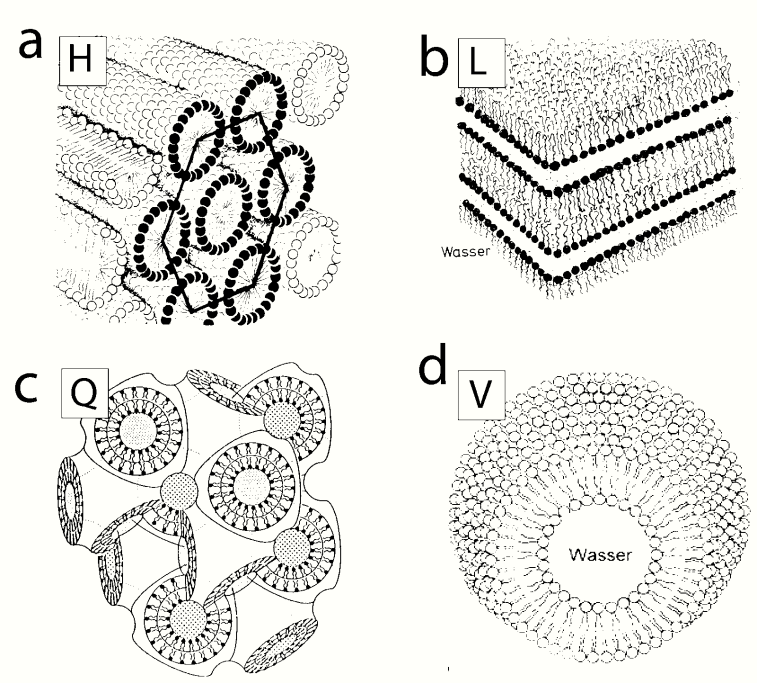

Figure 7.1: Some examples for possible lipid phases with increasing water content in the mixture from (a) to (d). (a) Hexagonal (H) phase with tubular, tightly packed lipids. (b) Lamellar phase with lipid bilayers (L) forming with small amouts of water betwen the layers.(c) Cubic phase with water enclosed in small voids in the lipid structure (Q). (d) Lipids vesicles (V) at infinite dilution and water content approaching 99%. Water is enclosed in spherical shells composed of a single lipid bilayer.

Vesicles form if the water content of the lipid containing solution is approaching 99%.

7.2.1 Simple argument for the shape

As already mentioned Bilayers consist of amphiphilic molecules. An amphiphile is charcterised by three parameters:

1. The head area a_0. This results from a balance of repulsions between the surfactant molecules (electrostatic, excluded volume, etc), and an effective attraction to minimise the contact area of hydrocarbon tails with water.

2. The critical chain length l_c. This is the maximum length of the hydrocarbon chain if stretched.

3. The hydrocarbon volume v. This is the volume occupied by the chain, irrespective of the conformation.

Here, we quickly recap the main arguments for the assembly of amphiphiles into different shapes.

Sphere
Consider a spherical micelle of radius r containing M molecules. Its volume is $V = \frac{4}{3}\pi r^3$ and also $V = Mv$. The surface area is $A = 4\pi r^2 = Ma_0$. This sets the condition that $r = \frac{3v}{a_0}$. In order for the sphere to be physically possible the radius has to be less than the critical length: $r < l_c$. These conditions are summarized as:

$$\boxed{\frac{v}{l_c a_0} \leq \frac{1}{3}}. \tag{7.1}$$

Cylinder
A similar argument to the one for spheres gives the the upper limit $\frac{1}{2}$ in this relation:

$$\boxed{\frac{1}{3} \leq \frac{v}{l_c a_0} \leq \frac{1}{2}}. \tag{7.2}$$

Bilayer
Bilayers are preferred if

$$\boxed{\frac{v}{l_c a_0} > \frac{1}{2}}. \tag{7.3}$$

then the geometry of the amphiphile favors the formation of bilayers (a planar or gently curved membrane). This condition means that for a given optimal a_0, the volume is large and the critical length is small. This is achieved in practice by molecules with a double hydrocarbon chain, like biological phospholipids. A bilayer can join its edges together to form a vesicle, gaining some edge energy but at a cost that comes from bending the bilayer.

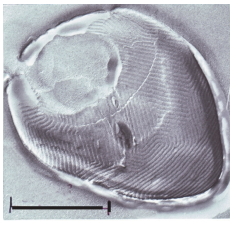

Figure 7.2: Electron microscopy image of a lipid vesicle in the ripple phase. Scale is 10 microns.

7.2.2 Membrane phase transitions

Planar or curved lipid bilayers (for example in vesicles) can also exist in different phases as shown in Figure 7.3. There are three main states called L_α, L_β and P_β. All three are found in biological systems.

At temperatures above the melting transition T_m, the L_α the carbon chains in the tail groups are disordered. In this phase the lipids are relatively free to move as the head groups are spaced and the tails are disordered. This state is the fluidic phase as shown on the left in Figure 7.3. If the temperature is lowered the carbon groups become stretched and the head groups are forced together in the P_β phase or ripple phase shown in the middle panel in Figure 7.3. The lowest energy configuration is the L_β phase where the tails are tilted, the membranes is tightly packed and thinner that in L_α.

The angle γ of the tilt for L_β and P_β is determined by geometric parameters given by the areas of the head group and tails. Since the lipids are much more confined in L_β and P_β both are often also denoted as quasicrystalline. On some of the quasicrystalline phases the lipid membrane actually exhibits a three dimensional structure with undulations to relax internal stress. An electron microscopy image of the P_β state is shown in Figure 7.2. At even lower temperature there is a second phase transition into L_β where the tails tilt and the membrane thickness is further reduced. L_β is also known as solid-ordered state. Sometimes L_β and P_β are also called gel-like to emphasize that lipids are equivalent to polymers below their glass transition temperature.

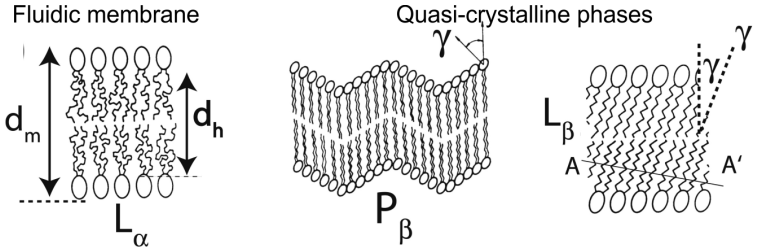

Figure 7.3: Molecular structures of lipid membranes in fluidic L_α (left) and two quasi-crystalline states P_β (middle) and L_β.

The phase transitions can be measured through differential scanning calorimetry and are indicated by changes in the specific heat capacity of the lipid vesicle containing solution Δc_P. A typical measurement for a DMPC membrane composed of only a single lipid is shown in $Figure$ 7.4. The three states L_β, P_β and L_α are indicated as well as the two transition temperatures, pre transition $L_\beta \leftrightarrow P_\beta$ at T_P, and main transition T_m at $P_\beta \leftrightarrow L_\alpha$, observable due to a clear change in c_p. The enthalpy corresponding to the transition can be deduced from the melting curve:

$$\Delta H = \int_{T_0}^{T_1} \Delta c_p dT \tag{7.4}$$

while the corresponding entropy is

$$\Delta S = \int_{T_0}^{T_1} \frac{\Delta c_p}{T} dT. \tag{7.5}$$

The last equation can be simplified if the melting transition is very sharp and resembles a delta function ($c_p/T \approx c_p/T_m$) one can define

$$\Delta S = \Delta H/T_m. \tag{7.6}$$

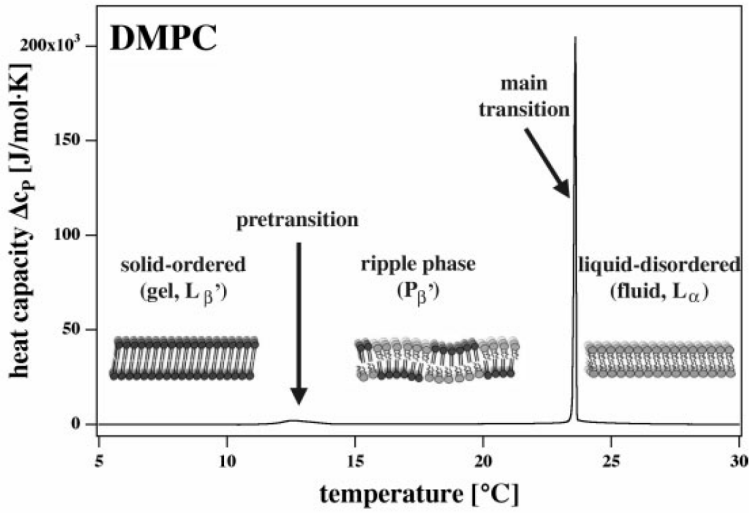

Figure 7.4: Calorimetric melting profile of dimyristoyl phosphatidylcholine (DMPC). The melting curve displays two peaks called pretransition at T_P and main transition at T_m. Below the pretransition one finds the solid-ordered phase or gel phase, between pretransition and main transition the ripple phase is found. Above the main transition one finds the liquid-disordered state (fluid phase). The ripple phase most likely is an intermediate between the gel and fluid phase.

7.2.3 Influence of pressure on phase transition temperature

The application of pressure shifts the phase transition temperature. This can be easily seen by going back to eq.7.6. For a sharp transition it follows

$$T_m = \frac{\Delta H_0}{\Delta S} = \frac{\Delta E_0 + p_0 \Delta V}{\Delta S} \tag{7.7}$$

at a constant pressure p_0. Increase of the pressure by Δp will change the enthalpy by $\Delta(\Delta H) = \Delta p \Delta V$ and thus the change in T_m is

$$\Delta T_m = \frac{\Delta p \Delta V}{\Delta S} = \Delta p T_m \frac{\Delta V}{\Delta H_0} \tag{7.8}$$

The changes are measurable at high pressures, experimentally T_m for DMPC is found to shift by roughly 1 K when the pressure is increased by 40 bar. A typical melting curve is shown in Figure 7.5 for DMPC.

By reordering the result for $\Delta T_m T_m$ one can calculate the volume change ΔV of the membrane as

$$\Delta V = \frac{\Delta T_m \Delta H_0}{T_m \Delta p} \tag{7.9}$$

where ΔH_0 and T_m are the values at atmospheric pressures. T_m depends roughly linear on the applied pressures up to 1000-2000 bar.

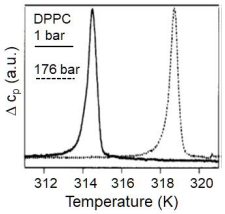

Figure 7.5: Change in heat capacity of DPPC when pressure is changed from 1 bar (solid line) to 176 bar (dashed line).

Experiments on a range of different lipids show shifts in T_m of similar magnitude within the experimental error. This result suggests that $\Delta V/\Delta H_0$ is independent from the exact type of lipid.

7.2.4 Micelles, Nematic, Hexagonal and Lamellar phases

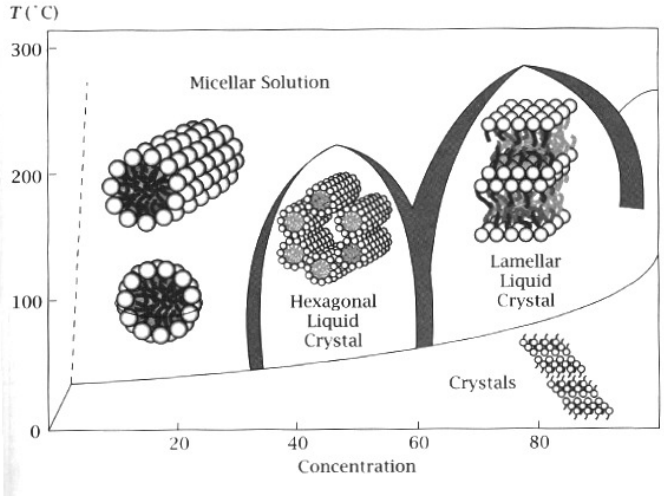

Figure 7.6: Amphiphiles at high concentration assemble to form different phases, depending on their geometry and also on the mechanical bending properties of the basic elements. These are typical examples of complex fluids, of practical (soaps) and technological (nanostructured materials) importance.

The balance of translational entropy versus curvature energies gives rise to very complex phase diagrams when the concentration of amphiphile is increased, see Figure 7.6. At sufficiently high concentrations, the interactions between the assembled structures themselves will begin to play a role as well. With the further complication of extending these ideas to more than a single component, this approaches the complexity of real world biological structures, and also forms the basis on which detergent and personal care products are formulated.

7.3 Soft Membranes

There are important examples of all of the shapes described above for the self assembly of amphiphiles. For example, spherical micelles are a fundamental structure in milk; cylindrical micelles can exist in a dense form that is very important technologically, known as entangled wormlike micelles. Inside a biological cell, the bilayer is certainly the most common motif, present either as extended flat

sheets, or curved, closed-up vesicles. This section will look more closely at the physical properties of bilayers, and describe qualitatively the importance of membranes within cells.

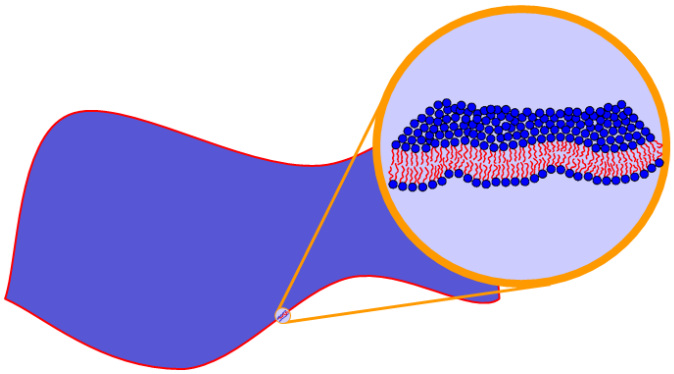

Figure 7.7: Diagram of amphiphiles assembling into a bilayer. The typical thickness of a biological membrane is around 30-40Å for phospholipids depending on the number of carbon atoms in the hydrophobic chain and the phase.

7.3.1 Membrane fluctuations in the Helfrich model

This section were adapted from the lecture notes of Prof Marcus Deserno and Prof Pietro Cicuta.

A physical description of a membrane requires us to know how its energy changes when we do something to it. Stretching and shear deformations have been introduced in an earlier chapter[1].

The shear modulus of membranes is very hard to measure directly. It is usually measured indirectly, in combination with other properties, by performing deformations that involve both bending and shearing. For bilayers of phospholipids, there is usually a completely negligible elastic shear modulus, and only a shear viscosity, i.e. phospholipid bilayers are two dimensional fluids. Two-dimensional not in the strict mathematical sense, but in the physical sense of motion and structure being confined to a surface. A membrane also has an important mode of deformation, bending, which is independent of shear and stretching. In bending a bilayer, the average area per molecule does not change, and the lipids don't have

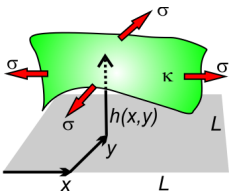

Figure 7.8: Diagram of a membrane with a planar average shape, and only small bending deformations, subject to a tension σ.

[1]The stretching modulus $K_{stretch}$ can be measured experimentally, for instance in micropipette experiments. Membranes can exist tension-free or under tension. A typical source of tension can arise if the membrane is enclosing a volume of fluid with a higher osmotic pressure when compared to the outside. If the membrane is under tension, the force required to hold it and pull it is proportional to the tension. The tension and the stretching modulus act in the same way, and have the same units, but while the modulus is a property of the material itself, the tension is a property that depends on the system conditions.

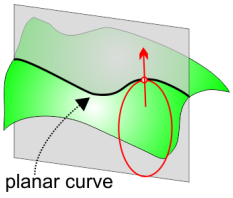

Figure 7.9: Diagrams showing that the curvature of a 2d surface has to be characterised by two numbers.

to rearrange their positions in the layer. The effect of bending is to induce tilt and splay between the phospholipid molecules. This is at the origin of the bending energy.

We will consider here only a simple case, of a membrane with a planar average shape, and only small deformations, as sketched in Figure 7.8. These deformations will clearly increase the membrane area relative to the plane (i.e. stretch), and also induce a curvature. We still have not defined what is the strain, for the case of bending. Being a two-dimensional surface, there are various types of bending that could be going on at a single point, and we need to look at this in a bit more detail, see Figure 7.9. The mathematical language in which this is properly discussed is differential geometry. We will limit the treatment to very simple cases, but you should be aware that this is a very well developed part of soft matter physics.

7.3.2 Surface deformations in Monge parametrization

Deformations cause stretch

Consider a point P on a surface embedded in 3d, as in Figure 7.8, with coordinates $P = (x, y, h(x, y))$. A point P_x a distance dx in the x-direction has the coordinates $(x + dx, y, h(x + dx, y)) \simeq (x + dx, y, h(x, y) + h_x(x, y)dx)$, where $h_x = \partial h/\partial x$. The vector $\overrightarrow{PP_x}$ is approximately $(1, 0, h_x)dx$. We can do the same consideration for a point P_y a distance dy in the y direction. The vectors $\overrightarrow{PP_x}$ and $\overrightarrow{PP_y}$ span a parallelogram, whose area dA is equal to the modulus of the cross product between these vectors:

$$\begin{aligned} dA &= \left| \begin{pmatrix} 1 \\ 0 \\ h_x \end{pmatrix} dx \times \begin{pmatrix} 0 \\ 1 \\ h_y \end{pmatrix} dy \right| = \left| \begin{pmatrix} -h_x \\ -h_y \\ 1 \end{pmatrix} dxdy \right| = \\ &= \sqrt{1 + h_x^2 + h_y^2}\, dxdy = \sqrt{1 + (\bigtriangledown h)^2}\, dxdy. \end{aligned} \tag{7.10}$$

For small displacements h relative to the average membrane plane $z = 0$, the area of a surface element can be obtained by expanding eq. 7.10:

$$\boxed{dA = \left(1 + \frac{1}{2}(\bigtriangledown h)^2\right) dxdy} \tag{7.11}$$

The actual increase in the infinitesimal area element arising from the deformation (relative to the plane) is $dA - dxdy$. This approximation, eq. 7.11, is of a form that can be treated easily analytically (but larger deformations require much more complex differential geometry).

Deformations cause curvature

For a simple curve the curvature at a given point P has a magnitude equal to the reciprocal of the radius of an osculating circle, i.e. a circle that closely touches the curve around the given point. Curvature is sometimes considered as a vector, pointing in the direction of that circle's center. The smaller the radius r of the osculating circle, the larger the magnitude of the curvature $(1/r)$ will be; a nearly straight curve has curvature close to zero; a circle of radius r has curvature $1/r$ everywhere.

When considering a curve drawn on a surface, one cannot readily identify the curvature of the curve with the curvature of the surface. First one has to disentangle these two different contributions. The trick is to look at two (unit) vectors: One is the local normal vector $\hat{n}$ of the surface, and the other is the principal normal $\hat{p}$ of the curve, i.e. the direction in which the curve locally curves.

The local curvature of the curve multiplied by the scalar product between the two normal vectors, $\hat{n} \cdot \hat{p}$, is a curvature that no longer depends on any property of the curve, except its direction. This resulting curvature is called the directional curvature. At every point, a surface has a directional curvature in each direction. Since there are infinitely many directions, there may also be infinitely many curvatures. It turns out that there are always two directions, and they are even orthogonal (but not necessarily unique), in which the directional curvatures are extremal. These directions are called principal directions, and the corresponding curvatures are called principal curvatures:c_1 and c_2. Two important combinations of these are:

$$\begin{aligned} H &= \frac{c_1 + c_2}{2} \quad \text{mean curvature} \\ K_G &= c_1 c_2 \quad \text{Gaussian curvature} \end{aligned} \tag{7.12}$$

Relating these considerations to the case of the 2d surface described by coordinates $P = (x, y, h(x, y))$ is not at all trivial. It is much simpler to see (this is a good exercise, simple geometry) that in 1d the curvature is related to the function that describes the curve by:

$$H = \frac{1}{r} = \frac{f''(x)}{(1 + f'(x)^2)^{\frac{3}{2}}} = \left(\frac{f'(x)}{\sqrt{1 + f'(x)^2}} \right)' \simeq f''(x) \tag{7.13}$$

where the final approximation is for small gradients: $|f'| << 1$.

A similar formula applies in 2d:

$$\boxed{H \;=\; \frac{1}{2}\nabla \cdot \frac{\nabla h(\mathbf{x})}{[1+(\nabla h(\mathbf{x}))^2]} \;\simeq\; \frac{1}{2}\nabla^2 h(\mathbf{x})} \tag{7.14}$$

If the membrane spans a quadratic frame of size $L \times L$, the total increase in energy due to the work against membrane tension σ (stretching the membrane) and bending the membrane is given (to first order) by:

$$\begin{aligned} \delta E &= \delta E_\sigma + \delta E_B \\ &= \sigma \int_0^L \int_0^L \frac{1}{2}\left[\left(\frac{\partial h}{\partial x}\right)^2 + \left(\frac{\partial h}{\partial y}\right)^2\right] dxdy + \\ &+ \kappa \int_0^L \int_0^L \frac{1}{2}\left[\frac{\partial^2 h}{\partial x^2} + \frac{\partial^2 h}{\partial y^2}\right]^2 dxdy \end{aligned} \tag{7.15}$$

The membrane will try to minimise the free energy of eq. 7.15, given the boundary conditions.

7.3.3 Spectrum of fluctuations

An important problem is to consider the shape of a membrane described by eq. 7.15 when it is subject to thermal noise. To proceed further in this problem, and in many others with a similar mathematical structure, it is useful to consider Fourier-expanding the displacement field, in this case the membrane shape $h(\vec{r})$. We assume for convenience periodic boundary conditions, so that the shape can be expanded in Fourier integral:

$$h(\vec{x}) \;=\; \frac{A}{(2\pi)^2}\int d\vec{q}\,\tilde{h}_{\vec{q}}\, e^{i\vec{q}\vec{x}}. \tag{7.16}$$

Note that this is a 2d transform, and that the area A in the numerator is $A = L\times L$.[2] The inverse transform is:

$$\tilde{h}_{\vec{q}} \;=\; \frac{1}{A}\int d\vec{x}\, h(\vec{x})\, e^{-i\vec{q}\vec{x}}. \tag{7.17}$$

[2]For a finite area, we should have used the Fourier series. What has been done is to consider the continuum limit, where the discrete nature of the mode numbers becomes irrelevant. Then the Fourier series becomes an integral, taking care to put the correct mode density as the integrating measure.

We then get from Eq. 7.15 + Eq. 7.16:

$$\begin{aligned}\delta E &= \frac{A^2}{2}\int dx \int dy \Bigg\{ \sigma \Bigg[\left(\int \frac{d\vec{q}}{(2\pi)^2} (iq_x) h_{\vec{q}} e^{i\vec{q}\vec{x}} \right)^2 + \\ &+ \left(\int \frac{d\vec{q}}{(2\pi)^2} (iq_y) h_{\vec{q}} e^{i\vec{q}\vec{x}} \right)^2 \Bigg] + \\ &+ \kappa \left[\int \frac{d\vec{q}}{(2\pi)^2} (-q_x^2) h_{\vec{q}} e^{i\vec{q}\vec{x}} + \int \frac{d\vec{q}}{(2\pi)^2} (-q_y^2) h_{\vec{q}} e^{i\vec{q}\vec{x}} \right]^2 \Bigg\}. \end{aligned} \tag{7.18}$$

Knowing that the membrane surface $h(\mathbf{r})$ is a real function, the complex Fourier modes must satisfy the condition $h(\mathbf{q}) = h^*(-\mathbf{q})$, so eq. 7.18 can be simplified to:

$$\delta E = \frac{A^2}{2\,(2\pi)^2} \int d\vec{q} \Big\{ \sigma \left(q_x^2 + q_y^2 \right) + \kappa \left(q_x^2 + q_y^2 \right)^2 \Big\} h_{\vec{q}}^2. \tag{7.19}$$

From equipartition of this energy into modes $\vec{q}$, we expect[3]:

$$k_B T = \frac{A}{2} \left\{ \sigma q^2 + \kappa\, q^4 \right\} \langle h_{\vec{q}}^2 \rangle \tag{7.20}$$

where we have simplified the notation by using $q^2 = q_x^2 + q_y^2$.

Therefore (finally):

$$\boxed{\langle h_{\vec{q}}^2 \rangle = \frac{k_B T}{A} \frac{1}{\sigma q^2 + \kappa\, q^4}} \tag{7.21}$$

Note that the factors in front of the fraction on the r.h.s of eq. 7.21 depend on the Fourier transform convention that is chosen in eqs. 7.16 and 7.17. Giving a structure factor result, as the one in eq. 7.21 without specifying the Fourier transform would have little meaning.

Whether a particular undulation mode costs predominantly bending energy or tension energy is a question of the wave vector. For wave vectors smaller than $q_{crossover} = \sqrt{\sigma/\kappa}$, i.e. on large length scales, tension is the dominant energy contributing to eq. 7.21. Conversely, for wave vectors bigger than $q_{crossover}$, i.e. on small length scales, bending dominates.

[3]Note that $\frac{1}{2} k_B T$ and not $k_B T$ is given to each mode, even though there are two dimensions, to avoid double counting, given that the modes depend only on the modulus of q.

Eq. 7.21 is called the "fluctuation spectrum" or "static structure factor" of a membrane. It tells us the mean square- amplitude of membrane modes. Since they are thermally excited, they are also proportional to temperature. Importantly, the fluctuation spectrum depends on the bending modulus κ and on the applied tension σ. Measuring the fluctuation spectrum and fitting to eq. 7.21 is thus a viable method to extract the bending modulus in an experiment. The method is called flicker spectroscopy.

Average amplitude of fluctuations

What average undulation amplitude do we expect for the entire membrane, and not just for a single mode? The full membrane amplitude is the sum over all individual modes, and we can calculate that:

$$\begin{aligned} \langle h^2 \rangle &= \frac{A}{(2\pi)^2} \int_{q_{min}}^{q_{max}} dq 2\pi q \frac{k_B T}{A} \frac{1}{\sigma q^2 + \kappa q^4} \\ &= \frac{k_B T}{4\pi\sigma} \ln\left(\frac{q^2}{\sigma + \kappa q^2}\right) \Bigg|_{q_{min}}^{q_{max}} \\ &= \ldots \longrightarrow^{\sigma \to 0} \frac{k_B T}{16\pi^3 \kappa} A \end{aligned} \tag{7.22}$$

where we have introduced a large wavelength cutoff $q_{min} = 2\pi/L$ and a small wavelength cutoff $q_{max} = 2\pi/d$, where d is comparable to bilayer thickness. The final approximate relation gives rise to a nice rule of thumb: Since a very typical value for the bending stiffness is $\kappa \simeq 20 k_B T$, inserting it we find

$$\sqrt{\langle h^2 \rangle} = \frac{L}{100} \tag{7.23}$$

i.e., the root mean square amplitude of the membrane fluctuations under vanishing tension are typically about 1% of the lateral extension of the membrane. Of course, if the membrane is under tension, this value is reduced.

7.3.4 Biological cell membranes

Membrane vesicles, surrounded by a single lipid bilayer, are being created, moved, fused into other membranes during many biological processes. Phospholipid membranes are found as the outside barrier of the cells but also make up boundary for many organelles inside of cells. In the case of animals, the outer membranes is called plasma membrane. Plants have an additional cell wall outside the phospholipid bilayer that provides additional stability.

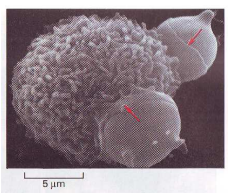

Figure 7.12: This electron microscopy image has captured a macrophage cell engulfing two red blood cells via the process of phagocytosis. The red arrows point to the leading edge of a mem-

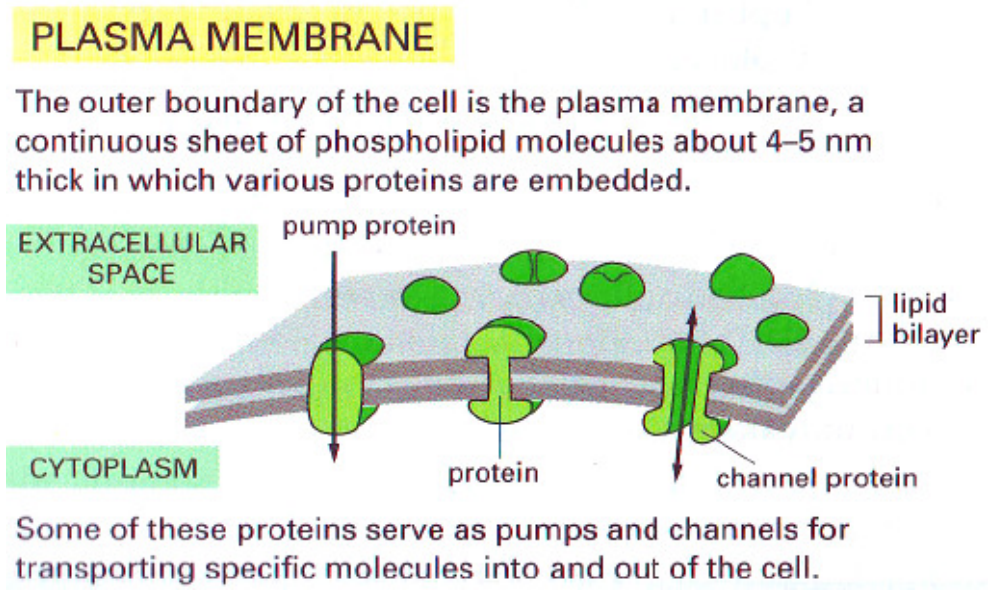

Figure 7.10: Simplified schematic of a biological plasma membrane composed of lipid bilayer containing membrane proteins. Membrane proteins may regulate transport of ions, water and other macromolecules. The varying thicknesses given for membranes is due to the broad range of possible lipids and may also differ when the first few water layers and (immobile) ions are included.

The energy related to curvature, and the intrinsic curvature of bilayers, are important in defining the shape of the biological membrane. Other important physical parameters of the membrane are its viscosity (fluidity) and its phase behavior. The viscosity of the membrane determines how fast objects confined to the membrane can move. Typical such "objects" are the membrane proteins, and assemblies of these proteins. Their function is to regulate membrane processes. For example there are pumps that regulate the concentration of calcium, potassium, pH, etc. across the membrane. There are membrane proteins that bind to specific chemicals, and trigger a particular response. The sequence of responses is called a signalling pathway. While many of these processes are very specific, and the details are different for each chemical pathway, this is also an area where general physical principles are important. We have already seen what it takes to bend a membrane; this energy needs to be found in order for example to "bud" a vesicle from the membrane.

The biological membrane is made not of one single phospholipid but by many hundreds of chemically different ones. In biological membranes, the composition of inner and outer leaflets in the bilayer is not the same. These multiphase systems have so many components that a complete phase diagram is impossibly complicated to measure. However there is a very important simplification. Phos-

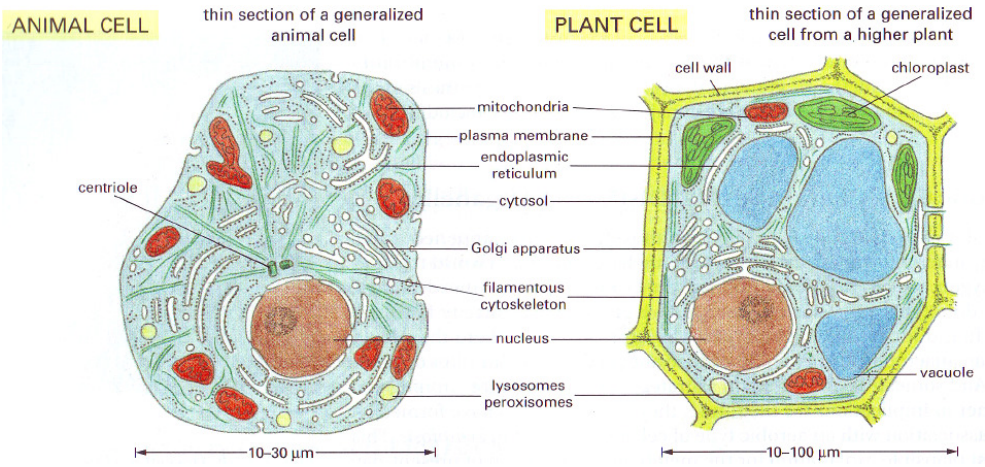

Figure 7.11: The diagrams show typical animal (left) and plant cells (right). Notice the many different organelles in both cell types that are surrounded by lipid membranes. The DNA is stored in the nucleus for both these eukaryotes. The plant cells are surrounded by a cell wall.

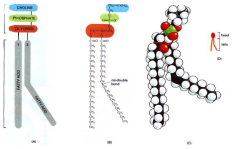

Figure 7.13: Unsaturated lipid.

pholipids fall into two classes: saturated and unsaturated. Figure 7.13 is a sketch of an unsaturated phospholipid. There is a kink in one of the fatty acid tails. A saturated phospholipid does not have that kink. Saturated lipids pack much more efficiently and with stronger order amongst themselves, giving bilayer phases with high viscosity. Unsaturated phospholipids pack with less order and have much higher mobility, hence the membrane has much lower viscosity. In many biological membranes there is roughly a ration of roughly 1:1 of saturated:unsaturated. There is also a high concentration of cholesterol, which is a smaller lipid that is "dissolved" in the hydrophobic layer. Such systems have a remarkably simple phase diagram, separating into two coexisting fluid phases at a temperature below 25^oC. There is active research aiming at establishing if and how the vicinity to the critical point is related to any biological role.

7.4 Self assembled structures

7.4.1 Biological examples: viruses

As long ago as 1955 it was shown that an infectious rodlike virus the tobacco mosaic virus could be reversibly reconstituted in the laboratory from a two component solution of its purified genome (RNA in this instance) and the protein that comprises its cylindrical capsid. Reversible self-assembly has been demonstrated as well for a number of spherelike plant viruses. In all of these cases, the assembly proceeds spontaneously, without involving any "fuel consumption" such as adenosine triphosphate hydrolysis.

The capsids of viruses are formed from a minimum number of gene products, given the small size of viral genomes. On this basis it is expected that spherical viruses should have the symmetry of regular polyhedra ("platonic solids") all of whose faces are identical perfect polygons. The largest shell of this kind is an icosahedron consisting of 60 equivalent subunits. Geometrical schemes can explain the general construction of icosahedral shells, and Aaron Klug (Cambridge, MRC) was awarded the 1982 Chemistry Nobel prize for related work:
http://nobelprize.org/nobel_prizes/chemistry/laureates/1982/klug-lecture.pdf
There have been recent attempts to describe the viral self assembly into different shapes within a free energy framework analogous to that used here for phospholipid assembly into micelles and membranes.

7.4.2 Self Assembly and Nanotechnology

As a result of self assembly, ordered structures form spontaneously. These products can be structured on very small lengthscales, the main physical limit being the mechanical rigidity under thermal forces. In Nature this type of self assembly is widespread, giving rise to materials as different as spider silk and opal shells. These have in common that they are self assembled, under ambient conditions, and highly structured. In biology these structures have developed to perform a function, and are highly optimised. Contrast spider silk with teflon fibers... these are processed under extremely harsh conditions, and the control over the structure (hence the overall properties) is not comparable to silk.
It is of course possible today to manipulate single atoms with STM... it is also possible to grow or etch materials with single atomic layer resolution. These techniques are at the heart of manufacturing modern electronics. They are still very far from producing nanoscale 3d structures. Controlling self assembly is one of the aims for research in "Nanotechnology".
One of the current most promising areas is the self assembly of block-copolymers. These are polymer chains made of two chemically different halves. Upon phase separation, they can form a wide range of structures (similarly to surfactants), displaying order at nanometer lengthscales. They will be described further in an advanced course.

7.4.3 Patterns

The type of self-assembly described up to here relies on tuning the interactions between molecular components, so that the free energy minima, i.e. *equilibrium*, corresponds to the desired structure. There is also a very different approach to structuring, that relies on tuning the system so that the *dynamics* of how the system evolves (for example during phase separation) leads to a structured state. There

are then ways, depending on the system, in which such structures can be frozen in.
A technologically important case is inducing phase separation of a polymer blend, so that droplets form and grow, but choosing the composition and temperature of the system so that the phase separation stops because of gelation of the continuous phase.
Many examples of patterns are the result of a system becoming unstable. The full equations describing the system are almost inevitably nonlinear, but in many cases the onset of instability can be described within a linear approximation. The pattern (or structure) that forms is the one that "grows" the fastest, out of all the possible unstable structures.

Chapter 8

Surface Energy

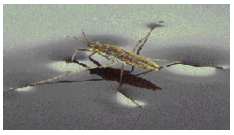

Figure 8.1: Water strider using surface tension.

8.1 Surface energy of liquids

8.1.1 Surface energy and tension

One of the most important intermolecular forces between molecules of the same species are the van der Waals (vdW) interactions. Usually vdW forces between molecules and atoms of the same kind are attractive. In liquids water and oil are in most cases immiscible since the intermolecular interaction between the same species is much stronger than for direct water-oil interactions.

These unfavorable interactions between molecules of different species (relative to molecules of the same species) lead to an energy penalty if one is to take a molecule from the bulk onto the interface (i.e. making a new piece of interface) or even removing it completely. The energy cost forces liquids that are in contact with each other to minimise their interfacial area within the geometrical constraints. The tendency of liquid phases to shrink to the minimum possible area leads to the formation of droplets. Typical examples are spherical oil droplets in suspension, or liquid droplets in sprays. The work required to create a new surface of area δA is

$$\delta E \; = \; \gamma \delta A, \tag{8.1}$$

which is an empirical definition of the surface tension γ. Typically surface tension is given in units of energy per unit area or force per unit length depending on the particular problem. Values for pairs of systems are $\gamma_{water/vapour} = 72 \times 10^{-3} N/m$ and for many oils (alkanes, etc) $\gamma_{water/oil} \simeq 30 \times 10^{-3} N/m$. Surface tensions can be changed and even brought very close to zero by the addition of surfactants. In case of water and oil mixtures these can be amphiphilic molecules. Other situations where surface tensions can reach very low values include phase separated

systems where the coexisting compositions are very similar. This happens, for instance, near the phase transition temperature or at the triple point for water where all phases are equally stable.
Surface tension can be measured using a microbalance, immersing either a "Wilhelmy plate" or a "Du Nuoy ring" in the interface and measuring the vertical component of the force. These methods work for tensions down to $\simeq 1 \times 10^{-3} N/m$, and other specialised instruments have been developed for situations that require even lower tensions to be assessed.

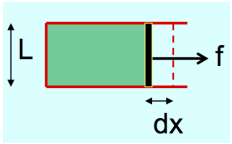

Figure 8.2: Stabilising an interface requires a counter balancing force.

8.1.2 Effects of surface tension

It is a general feature that liquids form spherical droplets. The spherical shape is a direct consequence of the surface energy as it maximises the volume while keeping the surface to a minimum. One way to visualise surface tension is to consider a two dimensional system as shown in Figure 8.2. An applied force f on the surface leads to a change in energy of

$$f dx = \gamma dA = \gamma L dx \tag{8.2}$$

$$\boxed{\gamma = f/L} \tag{8.3}$$

and can be used to see that γ has indeed units of Newton/m.

The additional free energy U required to move a molecule from the bulk to the surface can be also used to define γ. Thermodynamically we have

$$\gamma = \left(\frac{\partial U}{\partial A}\right)_{S,V,n_i} = \left(\frac{\partial F}{\partial A}\right)_{T,V,n_i} = \left(\frac{\partial G}{\partial A}\right)_{T,p,n_i} \tag{8.4}$$

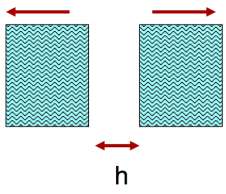

Figure 8.3: Separating two halves of liquid costs energy due to vdW interactions.

Within a continuum approach we can link γ to the vdW interactions and more specifically to the Hamaker constant A of the material. The connection between surface tension and vdW can be illustrated by calculating the force between two liquid slabs. We split a 'slab' of liquid in half (Figure 8.3) there will be a force $f(h)$ between the two parts that wants to minimise the surface energy. The force between the halves is due to the vdW interactions and given by

$$f(h) = \frac{A}{6\pi h^3}. \tag{8.5}$$

Typical values for the Hamaker constant are in the range of $A \approx 10^{-20}$ J. γ is then simply the integral

$$\gamma = \frac{1}{2}\int_a^\infty f(h)dh = \frac{A}{24\pi a^2}, \tag{8.6}$$

where a is the half the average distance between the molecules. Comparing this result with the expected γ for water one finds that these values are systematically too small. The reason for the underestimate is that we only considered static contributions. In fact, A is frequency dependent and for a correct treatment one would have to take the dispersion relations into account. However, in the context of this lecture the current treatment is more than adequate to link vdW interactions and surface tension.

8.1.3 Bubbles and droplets

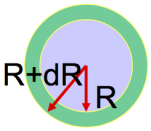

Figure 8.4: Increasing a droplet diameter and hence surface area requires energy.

With the introduction of surface tension we can now investigate droplets and bubbles. Starting with a droplet of radius R (Figure 8.4) that is expanded by dR the work is given by $\Delta p 4\pi R^2 dR$ where Δp is the pressure difference between inside and outside. In order to expand the droplet we need to increase the surface area and hence

$$\gamma \Delta A = 8\pi\gamma R dR = 4\pi \Delta p R^2 dR \tag{8.7}$$

and hence we are able to calculate the pressure difference

$$\Delta p = \frac{2\gamma}{R}. \tag{8.8}$$

As expected the pressure difference is positive with the resulting higher internal pressure. Interestingly, the pressure difference is twice as large for air bubbles (structures with thin water or soap shells and outer and inner medium air) as there is an inner and outer surface

$$\Delta p = \frac{4\gamma}{R}. \tag{8.9}$$

Often drops are not spherical and in those cases two radii need to be taken into account

$$\Delta p = \gamma \left(\frac{1}{R_1} + \frac{1}{R_2} \right). \tag{8.10}$$

Equation 8.10 is known as the Laplace disjoining pressure.

8.1.4 Capillary rise

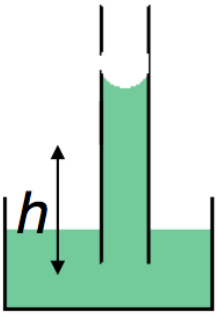

Figure 8.5: Water rising to height H in a thin capillary.

The rise of a water column (Figure 8.5) in a thin capillary can be modelled through the use of eq. 8.10. Hydrostatic pressure is increasing as liquid rises in the tube up to a maximum height h. The force acting on on the water column is $\rho g h$ and this has to be balanced with the increased pressure at the meniscus to reach equilibrium

$$\gamma \left(\frac{1}{R_1} + \frac{1}{R_2} \right) = \rho g h. \tag{8.11}$$

For a rotationally symmetric capillary we have $R_1 = R_2$ and hence get the result

$$\gamma = \frac{\rho g h R}{2} \tag{8.12}$$

This description works well if we can assume that the meniscus is indeed of uniform curvature and viscosity of the liquid is low. We also assume complete wetting and do not take into account the exact wetting angle at the meniscus that depends critically on the material parameters.

Given the density of a liquid ρ and its surface tension γ one can define the capillary length l_c

$$l_c = \sqrt{\frac{\gamma}{\rho g}} \tag{8.13}$$

which compares surface tension and gravitational force. For water $l_c \approx 2.7$ mm and droplets that are smaller or around adopt a near spherical shape that is not influenced by gravity. For small capillaries - a couple of mm in diameter - gravity does not change the shape of the meniscus significantly and eq. 8.12 holds and can be used to determine γ.

8.1.5 Amphiphiles at surfaces

We have introduced amphiphiles earlier in this course. These are molecules that have hydrophobic and hydrophylic groups, and therefore are particularly attracted to water/oil or water/air interfaces. It is possible for these molecules to be adsorbed to the surface so strongly that they have no chance to desorb. In this case they are called insoluble surfactants, and the concentration of surfactants on the surface does not need to be in any kind of equilibrium with the concentration in the bulk. There can even be no surfactants at all dissolved in the bulk.

Insoluble surfactants

It is possible to think of the surfactants on the surface as molecules confined to the plane, and the free energy per site is given by:

$$f \;=\; k_B T\big(\phi \log \phi \;+\; (1-\phi)\log(1-\phi)\big) + (\gamma_0 a^2 - u_0 \phi), \tag{8.14}$$

where we have considered excluded volume interaction, but no other forms of interaction, and γ_0 is the surface tension of the pure interface, a is the characteristic size of the surfactant molecules while u_0 is the energy gained by positioning a surfactant on the interface instead of in the bulk. There are $N_{sites} = A/a^2$, and

remember that the area fraction ϕ is a function of the area: $\phi = A_{surfactant}/A$. The surface tension (in the presence of the surfactant) is given by:

$$\begin{aligned} \gamma = \frac{\partial F}{\partial A} &= \ldots \\ &= \gamma_0 + \frac{k_B T}{a^2} \log(1-\phi). \end{aligned} \tag{8.15}$$

It is relatively straightforward to work though eq. 8.15 using $F = nf$. If the result of eq. 8.15 is expanded for low surfactant coverage, the limiting behavior of this equation shows that the surface tension is reduced compared to the clean interface by an amount which is the ideal gas pressure of a two dimensional gas[1]. Eq. 8.15 contains the correction to the ideal gas pressure from considering the excluded volume. It is correct to think of the surfactant gas as exerting a pressure (an osmotic pressure), and it is important to note that (counterintuitively) for these systems the degree of hydrophobicity, which will determine the parameter u_0, actually plays no role in the capacity of the surfactant to reduce the surface tension.

Soluble surfactants

If the surfactants are soluble, that means that the adsorbed concentration (i.e. the density in the surface film) will be in equilibrium with the concentration in the subphase. We can consider the Gibbs free energy of the whole system (bulk + interface), for which:

$$dG = VdP - SdT + \sum_i \mu_i dn_i + Ad\gamma. \tag{8.16}$$

In equilibrium $dG = 0$, and at constant P, T and using the Gibbs-Duhem equation, we get:

$$\sum_i n_i d\mu_i + Ad\gamma = 0. \tag{8.17}$$

If there are 2 components (1-solvent and 2-solute), then this becomes

$$-d\gamma = \frac{n_1}{A} d\mu_1 + \frac{n_2}{A} d\mu_2. \tag{8.18}$$

The n_i/A are surface excess quantities, and by careful definition of the 'surface' layer, the solvent excess can be set to zero. The bulk chemical potential of the dilute solute is simply $\mu_2 = \mu_0 + k_B T \ln c$, so this leads to

$$\boxed{\frac{n}{A} = -\frac{1}{k_B T} \frac{d\gamma}{d(\ln c)}}. \quad \text{Gibbs adsorption isotherm} \tag{8.19}$$

[1]There is no "gas" in the sense of a vapor! The dilute surfactant molecules have an osmotic pressure which is the same as that of a two dimensional gas.

This equation, known as the Gibbs adsorption isotherm, is useful experimentally to determine n/A, which is the number of adsorbed molecules per unit area. Its inverse, A/n is the area available per molecule. Eq. 8.19 has been derived under the approximation of dilute surface and bulk conditions. It is most common for this equation to hold up to the critical micelle concentration (CMC), so it's the aggregation into micelles that usually determines the upper limit of validity for eq. 8.19. Since above the cmc the concentration of monomers does not increase with further increase of total surfactant concentration, the tension stops decreasing. Finding the bulk concentration at which the surface tension stops decreasing is often the simplest way to measure the cmc of a surfactant.

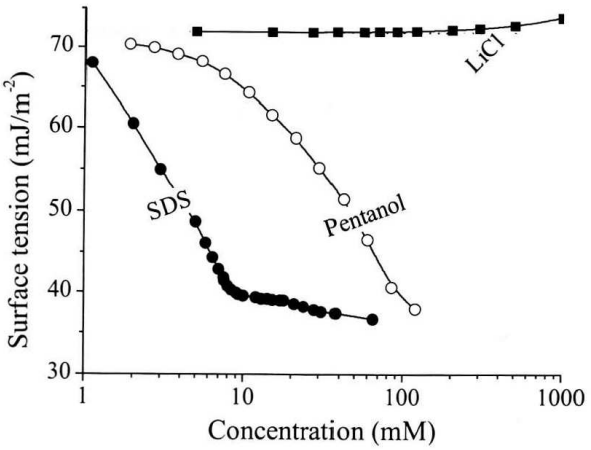

Figure 8.6: Experimental data showing the effect on the surface tension as a function of the concentration in the bulk, for three different solutes. SDS is a surfactant, n-pentanol an alcohol (a weak amphiphile), and LiCl a salt (lyophilic substance).

8.2 Wetting: Young's equation and contact angles

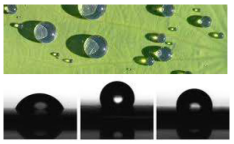

Figure 8.7: Top: Water droplets on a water-repellent leaf. Bottom: Droplets on hydrophilic, hydrophobic and intermediate surface.

The composition of the surface determines the interaction of water and thus the boundary conditions. In Figure 8.7 water droplets on different surfaces is shown. The shape is depending on the surface and the respective surface energies. These considerations are generally applicable and hold for any liquid in contact with any surface.

We have to take into account the relative surface energies (tensions) between all three constituents of droplet on a surface: liquid-surface (LS), liquid-vapour (LV) and surface-vapour (SV). A sketch of a droplet with the respective surface tensions is shown in Figure 8.8. Balancing the forces at the contact line where the solid, liquid and vapour meet is described by Young's equation:

$$\boxed{\gamma_{SL} + \gamma_{LV} \cos\Theta = \gamma_{SV}}\,. \tag{8.20}$$

For a complete wetting of the surface eq. 8.20 has no real solution for Θ. In this context one can sometimes find the wetting parameter defined as $S = \gamma_{SV} - (\gamma_{SL} + \gamma_{LV})$. S measures the difference in energy between a wet and dry solid substrate. If $S > 0$, the liquid spreads completely as this lowers its energy:

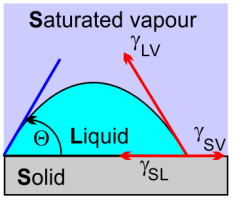

Figure 8.8: Contact angle Θ of a droplet on a surface is depending on the balance of the three surface tensions γ_{LV}, γ_{LS} and γ_{SV}. The saturated vapour ensures steady state.

$$\cos\Theta = \frac{\gamma_{SV} - \gamma_{SL}}{\gamma_{LV}}\,. \tag{8.21}$$

In any case when the fraction is larger than 1, Θ is 0 and we have complete wetting. For any values smaller than 1, Θ is finite and one observes partial wetting with a finite contact angle. If the fraction is -1 or even lower then $\Theta = 180°$. In this case no wetting occurs and - if gravity can be neglected - a perfect sphere forms on the non-wetting surface.

Usually, aqueous liquids spread on highly polarisable surfaces like (clean) glass or metals. On plastic materials it depends if the liquid is less polarisable than the polymer material. If surfaces are contaminated with hydrocarbons or other adherent molecules, the contact angle can change completely. One measures a wide range of contact angles for a given material if it is not cleaned properly.

The contact angle can also be controlled by the surface structure and roughness of the surface. Plants and animals have small pillars on tehir surface that effectively increase the contact angle. The pillars keep the water far from the surface and hence it cannot gain energy by wetting due to the larger surface area that needs to be covered. Hence, a droplet only touches parts of the surface. Examples are shown in Figure 8.9.

It is helpful to familiarize yourself with the concepts of hydrophobicity and hydrophilicity, and examples of solids of each type, the respective boundary conditions and forces acting at the surface.

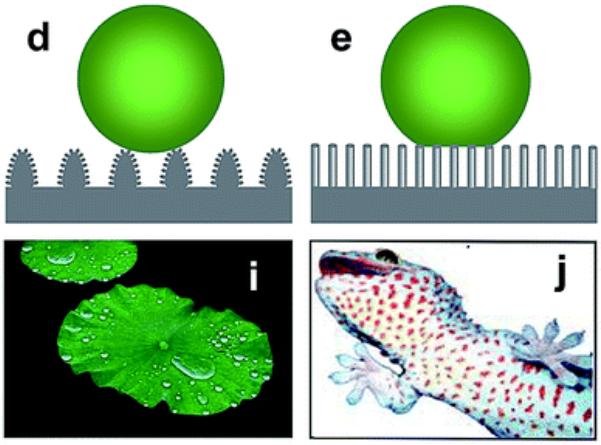

Figure 8.9: Micro and nanostructures decrease the contact angle in plants and animals. Shown are examples of a leaf and an animal with the respective structures found on their surfaces.

Chapter 9

Colloids, electrolyte solutions and charged interfaces

Parts of this chapter are based on lecture notes by Pietro Cicuta.

9.1 Definitions and Fundamentals

The encyclopedia Britannica defines colloids as: ”Colloid, any substance consisting of particles substantially larger than atoms or ordinary molecules but too small to be visible to the unaided eye; more broadly, any substance, including thin films and fibres, having at least one dimension in this general size range, which encompasses about 10^{-7} to 10^{-3} cm. Colloidal systems may exist as dispersions of one substance in another - for example, smoke particles in air or as single materials, such as rubber or the membrane of a biological cell.” As such, all materials investigated in this course can be regarded as colloids. At the same time colloids are of great industrial importance as they appear in many production processes, gels, creams or pastes and many other complex formulations are based on or contain colloids. In this lecture we will investigate the interactions between single colloidal particles. An understanding of the interactions between colloidal particles is essential for stabilising these suspensions and prevent aggregation due to mainly the van der Waals interactions. For soft matter science colloids are an ideal model system due to the high level of control over the shape and interactions between the particles. Thus colloidal system are also ideally suited to study general soft matter phenomena.

9.1.1 Examples of colloids

Typical examples of colloids include a suspension of particles that can be made form silica, gold and other metals, carbon (fullerenes), or polymers like PMMA and polystyrene. In natural systems colloids can be virus particles or the platelets found in clay. Thus colloids come in a wide range of different shapes, from spherical to rod-like, platelets. Since a few years even complex shapes like colloidal stars can be fabricated and their crystallisation is investigated. A correct description of the interactions requires a combination of Poisson-Boltzmann description of the electric double layer as well as the van der Waals forces. In addition due to the scale of the particles with respect to the solvent we need to consider excluded volume effects, osmotic pressure and also depletion interactions. As given in the encyclopedia definition above, colloids are often defined by the size of the constituent particles. However, a definition spanning four orders of magnitude seems not extremely helpful. Another possibility definition of a colloid is through a number characteristic properties and phenomena. Ideally we want to be able to disregard their atomic structure as much as possible. One example is a virus particles like the rod-like tobacco mosaic virus (TMV). TMV has an extremely complex structure but we will only need to know the shape (rod), its overall charge and the flexibility to describe its properties as a colloid.

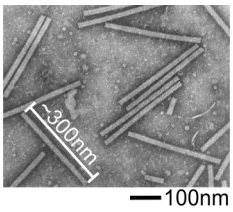

Figure 9.1: Electron microscopy image of the tobacco mosaic virus. The fully assembled virus has a length of 300 nm and diameter of 15 nm.

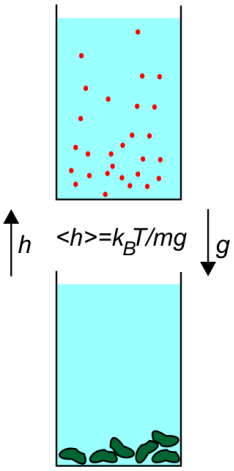

Figure 9.2: The 'gravitational length' $< h >= K_BT/mg$ of colloids (top) and pebbles (bottom) suspended in water. Thermal energy allows the colloidal particles to move.

9.1.2 Colloids and thermal energy

We will use statistical mechanics to describe colloids and thus our relevant energy scale is k_BT. We are interested in the properties that arise form colloidal particles having access to more than one configuration. In a suspension we can compare the thermal energy with the gravitational force mgh on a colloidal particle. The distribution of colloids follows the barometric distribution as

$$P(h) = \exp\left(\frac{-mgh}{k_BT}\right) \tag{9.1}$$

In a colloid $< h >$ should be larger than the particle size. In other words a pebble is no colloid. For a typical colloidal particle one finds $3k_BT/4\pi\rho g = R^4$ and thus $R \approx 1$ μm. Only if the particle can diffuse over a distance given by their radius during an experiment the physics becomes interesting. For a typical colloidal particle with diameter of 1 μm in water the diffusion time is around 1 s. In biological systems one can see proteins, viruses and bacteria as colloids, while larger cells are not.

9.1.3 Relevant forces of interaction

In the following we will discuss the five relevant forces acting between particles: (i) excluded volume interactions that are a consequence of the Pauli exclusion principle and the finite size of the colloids. Colloids do not overlap. (ii) Further we will look at dispersion forces, i.e. van der Waals interactions as discussed earlier. (iii) Colloidal particles in solvents are usually charged and hence we have to include Coulomb interactions. (iv) we need to take into account depletion interactions if the solvent cannot be treated as point-like particles. (v) finally if the particles are coated themselves with polymers by covalent bonds steric repulsion due to the excluded volume of the polymer chains leads to another possible way to prevent aggregation. The solvent can usually be described as a continuous medium that only has the effect of modifying the range of the five interaction forces.

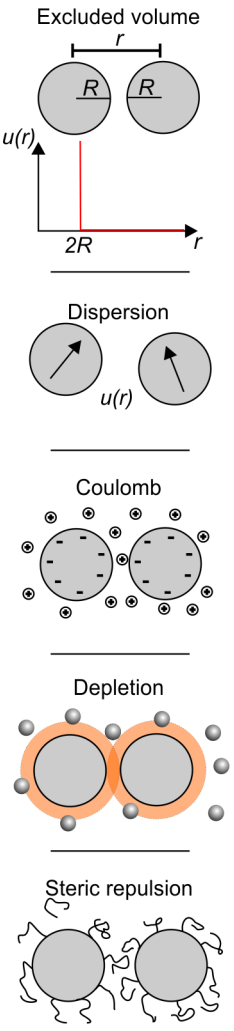

Figure 9.3: Forces of interactions between colloidal particles.

9.2 Interactions between colloidal particles

There are many types of interaction between objects in solution. Except for gravity, which does play a role in some colloidal systems, all the other interactions are of electrodynamic origin. For historical and practical reasons they have various different names. **Excluded volume** interactions are self explanatory. The force resisting overlap of two molecules is practically infinite in magnitude. **Covalent bonds** (energies between 100 and 300 k_BT) and weaker **hydrogen bond** (5 to 30 k_BT and specific to water) can exist between specific pairs of atoms, and have been studied in chemistry courses. **Coulomb interaction** is also very strong, at least in a vacuum. Exercise: calculate *in a vacuum* the binding energy for a pair of opposite monovalent ions, at a typical separation of 0.28nm. Answer: Around $200k_BT$, so of the same order of magnitude as a covalent bond. Indeed, as we know well, salt molecules like sodium chloride are very stable in air. In water, the Coulomb interaction between isolated ions is much reduced, because the relative dielectric constant is very high ($\epsilon = 78$, we will often simply use $\epsilon \approx 80$ throughout the course). In the presence of a finite concentration of dissolved ions, the interaction between ion pairs is further modified. The dissolved ions screen the interaction, and the effective law is not of Coulomb's form any more. Another interaction which is specific to water is known as **hydrophobic interaction**. This acts at very short range and involves orientation of water molecules near a nonpolar material, with a corresponding loss of entropy relative to a freely rotating water molecule. **Dispersion forces**, due to induced dipole-induced dipole interactions, are present between all pairs of atoms, and play an important role in soft materials.

We now consider in greater detail some of these interactions.

9.3 Dispersion forces

The interaction between two molecules is described by force between them defined as

$$F(r) = -\frac{du(r)}{dr} \tag{9.2}$$

where $u(r)$ is the pair potential and r the distance between the pair of molecules. In general the molecules repel when they are close, attract each other at intermediate distances and do not interact at large distance. A direct consequence is that there has to be distance when the attraction and repulsion balance - hence a minimum has to exist. The intermolecular forces are thus very similar to forces in covalent bonds, just their bond-length might be considerably larger and is easily adjustable by outer parameters in the case of colloidal systems.

Further to the realisation that there has to be a 'bond' length, it is also helpful to consider the range of interactions. Any potential $u(r)$ scaling with r^{-1} is considered to be long-ranged while higher exponents result in short ranges interactions. The Coulomb interaction or gravity are the well-known examples of long-ranged interactions. Van der Waals and London forces are short ranges with exponents of up to r^{-6}. In soft matter we are most interested in the long-ranged attractive interactions as they control the stability of colloidal suspensions. The short-ranged repulsive forces are not explicitly modelled and often we will assume that particles and molecules are hard-spheres.

9.3.1 Electrostatic interactions and short-ranged attraction

Coulomb interactions are in first order long ranged but the exponent increases when more complex charge distributions are allowed, namely multipoles. Dipoles or quadrupoles are possible even in neutral molecules. In addition short ranged interactions are possible when molecules have dipoles that can freely orient themselves. A third possibility is that molecules are polarisable and hence interactions between the electron clouds through the Coulomb interactions lead to short-ranged attraction.

9.3.2 London and van der Waals

The dispersion forces (sometimes referred to as London) or van der Waals (vdW) interactions are present between all atoms and molecules. London dispersion

forces are for polarisable molecules. The induced dipole moment is

$$\mu_i = \alpha E \tag{9.3}$$

where E is the electric field and $\alpha(E)$ is the polarisability, that is frequency dependent and non-liner in very high fields. The induced dipole moment can lead to an attractive force between a neutral atom and a charged object. The force can be calculated as a sum between the attraction between the charged molecule Q and the induced opposite charge $-q$ in the neutral molecule and the repulsion of the like charge q part:

$$F(r) = -q\left[E\left(r - \frac{\Delta r}{2}\right) - E\left(r + \frac{\Delta r}{2}\right)\right] \approx q\Delta r\frac{dE}{dr} = \mu_i\frac{dE}{dr}. \tag{9.4}$$

For standard Coulomb E scales a Qr^{-2} and with $\mu_i = \alpha E$ we get

$$F(r) = -2\alpha\left(\frac{Q}{4\pi\epsilon_0\epsilon_r}\right)^2\frac{1}{r^5} \tag{9.5}$$

and by integrating we can determine the potential $u(r)$

$$u(r) = -\int F(r)dr = -\frac{\alpha}{2}\left(\frac{Q}{4\pi\epsilon_0\epsilon_r}\right)^2\frac{1}{r^4}. \tag{9.6}$$

As Q is squared these interactions are always attractive.

Van der Waals interaction between polarisable molecules

Extending this now to two polarisable atoms one can obtain the vdW-interaction between two atoms. The vdW is of the form

$$V(r) \;=\; -\frac{2\alpha^2 h\nu}{(4\pi\epsilon_0)^2}\frac{1}{r^6}, \tag{9.7}$$

where α is the polarizability of the atom, h is Planck's constant and ν is the characteristic frequency of the electron's orbit around the nucleus (3.3×10^{15}Hz for the Hydrogen atom). Please note that this is the only place in the lecture where we use Planck's constant explicitly. These factors are shown here as a reminder of the quantum mechanical origin of the vdW interactions. In soft matter and biological physics and for the reminder of this course the form of eq. 9.7 the atomic parameters are summarised into one interaction parameter B (sometimes C or H are used instead):

$$V(r) \;=\; -\frac{B}{r^6}. \tag{9.8}$$

It is important to remember that the vdW interactions between a pairs of molecules decay extremely fast (r^{-6}). As we will see, these forces are important to understand the stability of colloidal systems that are composed of more than one atom or molecule. An atom or molecule within one colloidal particle interacts with all atoms or molecules in the other colloidal particle and hence these force of interactions are additive and hence will be long ranged. Any calculation of the dispersion forces between larger particles and assemblies needs to sum over all pairs of atoms. In a first approximation they can be considered as additive. There is an exercise in the question sheet where you work out how eq. 9.8 determines the interaction between two planar surfaces (solid blocks of material). The simpler case of the interaction between an atom and a surface is the basis for that calculation. Very similar calculations lead to sphere-solid and sphere-sphere interactions:

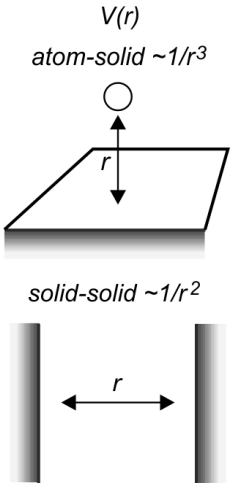

Figure 9.4: Scaling of interaction potential for different combinations of atom and solid.

$$V_{atom/solid}(r) = -\frac{\pi B\rho}{6r^3}. \tag{9.9}$$

$$V_{solid/solid}(r) = -\frac{A}{12\pi r^2} \text{ per unit area.} \tag{9.10}$$

$$V_{sphere/sphere}(r) = -\frac{\pi^2 B\rho^2 R}{12r} \text{ for } r \ll R. \tag{9.11}$$

Where ρ is the density of atoms, and A is a constant that depends on B and ρ, called the Hamaker constant that we use also in the section on surface tension 8.1. R is the radius of the sphere. Notice how in all these practical cases the range of interaction is increased substantially.

The long distance limit of eq. 9.11 returns to the atom-atom form of r^{-6}. These equations have been calculated for interactions in a vacuum. In a solvent, the functional form of the interaction remains the same, but the Hamaker constants and other prefactors need to be modified. One reason is the change of the polarizability of the solvent compared to vacuum.

For interactions between like atoms, the dispersion forces are almost always attractive. The attraction can lead to the aggregation and hence the destabilisation for colloidal systems. The influence of dispersion forces can be made to disappear by choosing a solvent with the same polarizability as the dispersed material. In practice this is often the same as choosing a solvent with the same polarizability as the colloids. It is interesting to note here that there exist materials where $A < 0$. In this case the atoms do not want to stay close to each other but rather maximise interactions with their environment. One such example is liquid helium that flows out of its container under certain conditions.

9.3.3 Quantum-mechanical argument for attraction among neutral molecules

This part of the lectures follows notes from Ray Goldstein.

One way to obtain a semi-quantitative understanding of the attraction between two polarizable (but neutral) molecules is viewing the problem as two linear springs: The Hamiltonian for the system is:

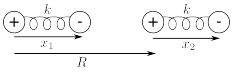

Figure 9.5: Two neutral molecules modelled as quantum mechanical harmonic oscillators.

$$\mathcal{H} = \mathcal{H}_0 + \mathcal{H}_1 = \text{Spring Energy} + \text{Coulombic Energy} \tag{9.12}$$

resulting in

$$\mathcal{H}_0 = \frac{p_1^2}{2m} + \frac{1}{2}m\omega_0^2 x_1^2 + \frac{p_2^2}{2m} + \frac{1}{2}m\omega_0^2 x_2^2 \tag{9.13}$$

and

$$\mathcal{H}_1 = e^2\left[\frac{1}{R} + \frac{1}{R - x_1 + x_2} - \frac{1}{R - x_1} - \frac{1}{R + x_2}\right] \sim -\frac{2e^2 x_1 x_2}{R^3}, |x_1|, |x_2| \ll R \tag{9.14}$$

To simplify the situation, a coordinate change is made:

$$x = \frac{x_1 \pm x_2}{\sqrt{2}} \tag{9.15}$$

$$x_1 = \frac{x_+ + x_-}{\sqrt{2}} \tag{9.16}$$

$$x_2 = \frac{x_+ - x_-}{\sqrt{2}} \tag{9.17}$$

and this results in

$$\mathcal{H} = \frac{p_1^2}{2m} + \frac{1}{2}\left(m\omega_0^2 - \frac{2e^2}{R^3}\right)x_+^2 + \frac{p_2^2}{2m} + \frac{1}{2}\left(m\omega_0^2 + \frac{2e^2}{R^3}\right)x_-^2 \tag{9.18}$$

The two terms in parenthesis are essentially adjusted frequencies:

$$\omega_+^2 = \omega_0^2 - \frac{2e^2}{mR^3} \tag{9.19}$$

$$\omega_-^2 = \omega_0^2 + \frac{2e^2}{mR^3} \tag{9.20}$$

and hence

$$\mathcal{H} = \frac{p_1^2}{2m} + \frac{1}{2}\left(m\omega_+^2\right)x_+^2 + \frac{p_2^2}{2m} + \frac{1}{2}\left(m\omega_-^2\right)x_-^2 \tag{9.21}$$

The energy is then:

$$U(r) = \frac{1}{2}\hbar\omega_+ + \frac{1}{2}\hbar\omega_- - 2\cdot\frac{1}{2}\hbar\omega_0 \approx \frac{-\hbar e^4}{2m^2\omega_0^2 R^6} \tag{9.22}$$

$$= \frac{-1}{2}\hbar\omega_0\frac{(e^2/m\omega_0^2)^2}{R^6} \tag{9.23}$$

$$= -\frac{1}{2}\hbar\omega_0\frac{(e^2/m\omega_0^2)^2}{R^6} \tag{9.24}$$

noting that $e^2/m\omega_0^2$ is a characteristic volume. Thus, the energy is related to the difficulty of polarizing the atom, as well as an effective volume. This can be checked using standard electromagnetics. The normal equation for magnetic displacement is:

$$\vec{d} = \alpha\vec{E} \tag{9.25}$$

The units on $\vec{d}$ are $Q\cdot L$, the units on $\vec{E}$ are Q/L^2, making the units of α L^3 (an effective volume). The Hamiltonian is:

$$\mathcal{H} = \mathcal{H}_0 + eE_0x_1 + eE_0x_2 \tag{9.26}$$

$$= \tfrac{1}{2}m\omega_0^2\left(x_1^2 + \tfrac{2eE_0x_1}{m\omega_0^2} \pm \left(\tfrac{eE_0}{m\omega_0^2}\right)^2\right) + (1\leftrightarrow 2) \tag{9.27}$$

$$= \tfrac{1}{2}m\omega_0^2 z_1^2 + \cdots \tag{9.28}$$

$$z_{1,2} = x_{1,2} + \tfrac{eE_0}{m\omega_0^2} \tag{9.29}$$

The dipole moment is then:

$$\alpha = \frac{e^2}{m\omega_0^2} \tag{9.30}$$

which is the same as seen previously. The energy of attraction in either case is then:

$$U(r) = -\frac{1}{2}\frac{\hbar\omega_0\alpha^2}{r^6} \tag{9.31}$$

9.4 Coulomb interactions for preventing aggregation

We established that the dispersion forces between colloids and basically all molecules or atoms are attractive - but of short range. The result of the attractive interaction is that colloids will aggregate over time. It is possible to change the dispersion forces by adding a solvent and reducing the range. However, on long time scales this still leads to aggregation as the diffusing colloids will eventually come close enough for vdW to dominate. As we cannot change the attractive interactions we need to exploit other forces to stabilise colloidal suspensions. In the following we will discuss how Coulomb interactions can be used to stabilise colloidal suspensions. Before we can discuss this we need to describe the interactions of ions with charged surfaces and the necessary changes to the Coulomb interactions.

9.4.1 Salt solutions and screened Coulomb interactions

Adding a small amount of salt like NaCl to water leads to dissolving the salt crystal. On a molecular level, the ionic crystal lattice is dissociating into positive Na^+ and negative Cl^- ions, each surrounded by a shell of water molecules. Although the resulting solution is overall neutral, the thermodynamic properties of such an electrolyte solution are fundamentally different compared to solutions of uncharged molecules. The ions in such electrolyte solutions are surrounded by counter-ions that neutralize their charge.

Before we start to consider electro-kinetic phenomena it is useful to discuss the key concepts of electrostatic interactions in electrolyte solutions containing charged objects like macromolecules or particles.

9.4.2 Dilute solutions

In a dilute electrolyte solution, all ions are completely dissociated. The i-th ions is described by charge $z_i e$. For example, the already mentioned monovalent ions sodium and chloride would have $z_{Na} = 1$ and $z_{Cl} = -1$. Since we require overall charge neutrality in all situations we have $\sum_i n_i z_i = 0$ where n_0 is the number density of the respective ion. Electrostatic interactions are long-ranged and hence ions are not randomly distributed in solutions. On average the distance between neighboring ions is the same, positive ions are more likely surrounded by negative ions than positive one. This leads to the formation of an effective ionic cloud of opposite charges surrounding each ion. The distribution of these ions is described by the Poisson Boltzmann equation. Before we discuss the PB equation it is useful consider Coulomb interaction energy in comparison to the thermal energy.

9.4.3 Bjerrum length

The electric potential $\phi(r)$ around a point charge is

$$\phi(r) = \frac{ez_i}{4\pi\epsilon_0\epsilon_r}\frac{1}{r} \tag{9.32}$$

In the following r may denote a vector or - for systems with rotational symmetry - a scalar. The electric field is the gradient of the potential and hence scales with $1/r^2$. Placing a second ion into the solution at distance r the energy is

$$U_{i,j}(r) = \frac{z_i z_j e^2}{4\pi\epsilon_0\epsilon_r}\frac{1}{r}. \tag{9.33}$$

Obviously the strength of the interactions depends on the distance and the valency z_i, z_j of the ions. By equating $U_{i,j}$ with the thermal energy k_BT we define the Bjerrum length l_B

$$l_B \equiv \frac{e^2}{4\pi\epsilon_0\epsilon_r k_B T} \tag{9.34}$$

l_B is the closest distance that two like-charged ions can have at a certain temperature. At $T = 300$ K one calculates $l_B \simeq 0.7$ nm for $\epsilon = 80$ as common for water. The Bjerrum length l_B is inversely proportional to the dielectric constant of the surrounding medium and hence is much longer in oils or even proteins where ϵ can be as small as 2.

9.4.4 Poisson-Boltzmann Equation

The ion distribution in the double layer is most commonly described within the so-called PoissonBoltzmann formalism.We first introduce a system with the very simple geometry

The system consists of a charged surface with a uniform surface charge density σ separated from a second, parallel surface that is electrically neutral. For most systems σ has a negative value; while this is not assumed in our derivation, the plots in the subsequent figures correspond to this case. The charged surface has a surface area A, and the surfaces are separated by a distance d. We assume that the lateral dimensions of the charged surface are sufficiently large that edge effects can be neglected; under these conditions all of the relevant equations become one-dimensional. The volume between the two planes is filled with an electrolyte, which is in diffusive equilibrium with a bulk reservoir. We take the electrolyte as consisting of water containing a number density n_0 of a fully dissociated monovalent salt. A good example of the latter is potassium chloride (KCl), which dissociates into K^+ and Cl^- ions.

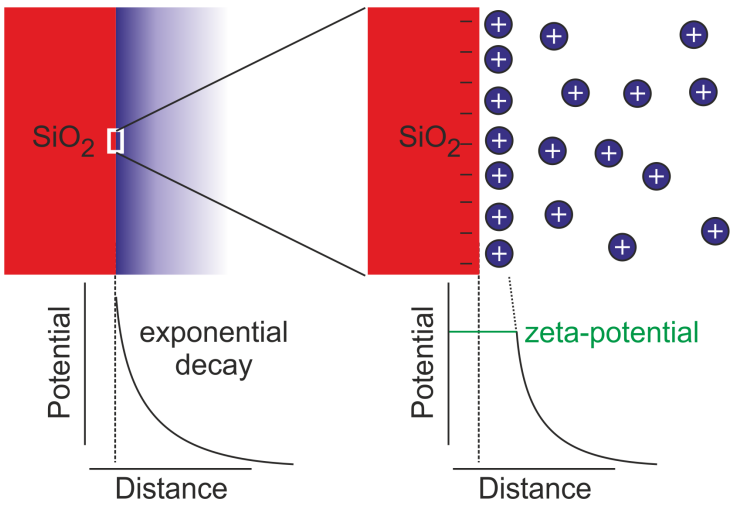

Figure 9.6: Screening layer above a charged wall in this example a negatively charged SiO_2 surface. Positive counter-ions (blue) of opposite charge to the charged surface screen the charges. The ion distribution with the surface is known as the electric double layer while the potential near the surface is known as ζ-potential. For clarity, water molecules and positive co-ions are not shown.

This implies that in bulk solution there is a number density n_0 of both positive ions (also known as cations) with charge $+e$ and negative ions (anions) with charge $-e$, where e is the charge of the electron. We treat water as a homogeneous medium with permittivity $\epsilon_w = 80\epsilon_0$. A uniform electric field with magnitude E is applied parallel to the surface and permeates the region between the surfaces. The direction perpendicular to the planes is x (with $x = 0$ corresponding to the position of the charged surface and $x = d$ to that of the neutral surface) and the direction along the planes is is defined as z. We will further assume that σ is small and that d is large, as defined more quantitatively below.

The electric potential $\phi(x)$ is defined by the the Poisson equation from electrostatics,

$$\nabla^2\phi(x) = \rho(x)/\epsilon_w, \tag{9.35}$$

where $\rho(x)$ denotes the local charge density. The charge density is connected to the ions:

$$\rho(x) = \sum_i ez_i n_i(x) \tag{9.36}$$

for i ions of charge $z_i e$. At equilibrium, the average concentration of charged molecules at position x follows the Boltzmann distribution,

$$n_\pm(x) = n_0 e^{\mp e\phi(x)/k_B T} \tag{9.37}$$

with $\phi(x)$ the local average potential and n_+, n_- as the local number densities of cations and anions, respectively. Here we assume $|z_i| = 1$ for both ions. We have

also introduced the convention that $\phi(x) = 0$ corresponds to the bulk reservoir far from any charged object, where $n_+ = n_- = n_0$.

Combining the Poisson equation and ρ for the ions results in:

$$\nabla^2\phi(x) = -\frac{e}{\epsilon_0\epsilon}\sum_i z_i n_{i0} \exp\left(\frac{-ez_i}{k_BT}\phi(x)\right) \tag{9.38}$$

where n_{i0} denotes the bulk concentration of ion i. It is important to point out at this point that the PB formula is not exact. One important correction is that the potential of mean force should be used instead of the average potential $\phi(x)$. Nevertheless, the PB formalism is very successful for describing many experimental results.

9.4.5 Debye-Hückel Equation

The PB equation is nonlinear and hence often requires numerical methods to solve. However, there are a number of cases where exact solutions can be found. One very powerful simplification os possible if we assume that $\phi(x)$ is much smaller than k_BT so that the Poisson-Boltzmann equation can be linearized,

$$\nabla^2\phi(x) = -\frac{e}{\epsilon_0\epsilon}\sum_i z_i n_{i0}\left[1 - \frac{ez_i}{k_BT}\phi(x)\right] \tag{9.39}$$

Since we require charge neutrality the first term in the sum vanishes and we obtain the the linearized PB euqation that is also known as Debye-Hückel equation:

$$\nabla^2\phi(x) = \kappa^2\phi(x) \tag{9.40}$$

where on can define the Debye-Hückel screening length $\lambda = 1/\kappa$ as

$$\kappa^2 \equiv \frac{e^2}{\epsilon_0\epsilon k_BT}\sum_i z_i^2 n_{i0} \tag{9.41}$$

l_D or λ is also known as the electrostatic screening length as denotes the distance from the charged surface when the potential falls to $1/e$. It shows that in electrolyte solutions the Coulomb interaction is screened reducing the range of the interactions.

There are important differences between l_B and λ. While λ is changing with the concentration of ions in the electrolyte, l_B is only set by the solution and thus unchanged.

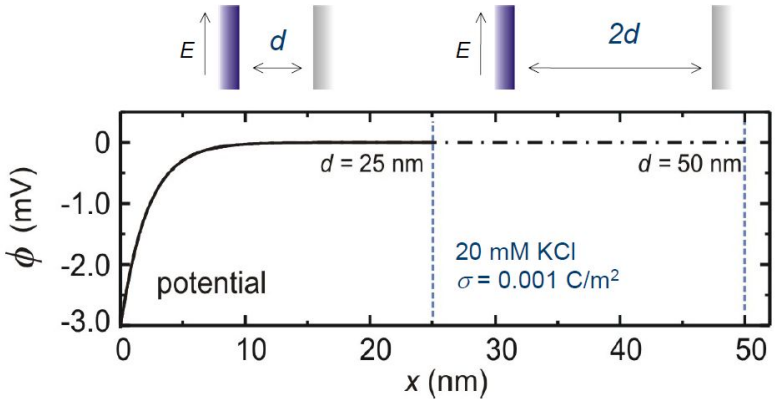

Figure 9.7: Two semi-infinite parallel plates are placed in salt solution at distance d and $2d$ as shown above. The left plate is charged (blue) while the right one is uncharged. Counter-ions lead to the formation of a double layer with an exponential decay as shown below. Below the resulting $\phi(x)$ is shown for d and $2d$. For $d \gg \lambda$ the potential is unperturbed by the uncharged plane. The parameters for surface charge σ and salt concentration are shown in the figure.

9.4.6 Charge and potential distribution between parallel plates

We will now look at a system consisting of two semi-infinite parallel plates with distance d and $2d$ as shown in Figure 9.7. For the linearized PB equation the number density of the ions follow Boltzmann factors for all ion types. In our specific example for two monovalent ions with charge $\pm e$ the concentration or number density n is given by:

$$n_{\pm}(x) = n_0 \left(1 \mp \frac{e\phi(x)}{k_B T}\right). \tag{9.42}$$

In order to determine self-consistently the electrostatic potential $\phi(x)$ we can now define $\rho(x) = e(n_+(x) - n_-(x))$. $\rho(x)$ is the local charge density above the charged surface. The result is a differential equation that can be solved for the electrostatic potential $\phi(x)$,

$$\frac{d^2\phi(x)}{dx^2} = \frac{2e^2 n_0}{k_B T \epsilon_w}\phi(x) = \frac{\phi(x)}{\lambda^2}. \tag{9.43}$$

Here and in the following $\epsilon_w = \epsilon_0 \epsilon$ for water. In the last step we introduced the Debye-Hückel screening length, $\lambda \equiv \sqrt{\frac{k_B T \epsilon_w}{2e^2 n_0}}$. [1]

[1] λ depends on fundamental constants and the salt concentration of the solution. It is important to remember that even pure water carries a low number of charges. For pure water one would expect a pH of 7 at room temperature equivalent to $10^(-7)$ M of H+ and OH^- ions which yields $\lambda \approx 1$ μm. For comparison, under typical physiological conditions found in biological systems (approximately 0.1 M of monovalent salt), $\lambda \approx 1$ nm, 1000 times smaller.

The general solution for this differential equation is $\phi(x) = Ae^{-x/\lambda} + Be^{+x/\lambda}$. To determine A and B we use the boundary conditions at $x = 0$ and $x = d$: $d\phi(0)/dx = -\sigma/\epsilon_w$ and $d\phi(d)/dx = 0$. The solution for the electrostatic potential is then

$$\phi(x) = \frac{\sigma\lambda}{\epsilon_w}\left(\frac{e^{-x/\lambda} - e^{-2d/\lambda + x/\lambda}}{1 + e^{-2d/\lambda}}.\right) \tag{9.44}$$

For $d \gg \lambda$ we get

$$\phi(x) = \frac{\sigma\lambda}{\epsilon_0\epsilon}e^{-x/\lambda}. \tag{9.45}$$

$\phi(x)$ is shown in Figure 9.7 for $d, 2d \gg \lambda$. Obviously this is only the case when the neutral wall is far enough from the charged wall to ensure that there is no influence on the charge distribution and $\phi(x)$. Our result shows that electrostatic interactions decay to zero in electrolytes over a characteristic distance λ.

In this example we assume low surface charge. In this case both charges can be present in the screening layer. In this limit the ions are distributed as Boltzmann factors as expected:

$$n_{\pm}(x) = n_0 \mp \frac{\sigma}{2e\lambda}e^{-x/\lambda}. \tag{9.46}$$

The net charge density in the diffuse layer is

$$\rho(x) = -\frac{\sigma}{\lambda}e^{-x/\lambda}. \tag{9.47}$$

Like the potential $\phi(x)$, the charge density $\rho(x)$ drops to zero with increasing distance from the charged surface with a decay length λ as the ions neutralize each other. Integration of this equation with respect to x also directly demonstrates that the total charge in the diffuse layer is equal and opposite to that of the surface being screened.

9.4.7 Some other geometries

The presence of the ions modifies the Coulomb interaction and reduces the range. It is instructive to calculate the Coulomb potential around a spherical charged object like an ion or colloidal particle. A calculation following similar steps can be done (in spherical coordinates) to work out the potential around a charged sphere of total charge Q and radius a:

$$\boxed{\psi(r) \;=\; \frac{Q}{4\pi\epsilon_0\epsilon_r r(1+\kappa a)}\exp\big(-\kappa(r-a)\big)} \quad \text{sphere} \tag{9.48}$$

With $a = 0$, eq. 9.48 yields the electrostatic potential due to a point-charge in a salt solution. Note that this is quite different from Coulomb's form that applies in solution without charge or in vacuum.

9.4.8 PB between plates with high surface charge

The above calculation holds so long as the surface charge density is sufficiently small that the condition $|\sigma| < k_B T \epsilon_w / e\lambda$ is satisfied. At higher surface charge densities, we have to solve the full Poisson-Boltzmann equation

$$\frac{d^2\phi(x)}{dx^2} = \frac{2en_0}{\epsilon_w} \sinh\left(\frac{e\phi(x)}{k_B T}\right). \tag{9.49}$$

Because of its non-linearity, this equation is considerably more difficult to solve. When $d \gg \lambda$, an analytical solution can nonetheless be obtained for the geometry with the two parallel plates

$$\phi(x) = \frac{2k_B T}{e} \ln\left(\frac{1+\gamma e^{-x/\lambda}}{1-\gamma e^{-x/\lambda}}\right) \tag{9.50}$$

with $\gamma = -\lambda_{GC}/\lambda + (1+\lambda_{GC}^2/\lambda^2)^{1/2}$. Here we introduced a new parameter $\lambda_{GC} = 2k_B T \epsilon_w / (e|\sigma|)$ which is known as the GouyChapman length. Qualitatively, λ_{GC} is a measure of the strength of the electrostatic interactions between ions and the surface, with a small λ_{GC} corresponding to strong interactions.

This result for $\phi(x)$ is shown in Figure 9.8 for a range of values of the surface charge σ. From bottom to top, the curves correspond to values of the surface charge density σ of 0.001, 0.003, 0.005, 0.01, 0.025, 0.05, 0.1, 0.5 and 1.0 Cm^{-2} in 20 mM KCl at 300 K. For low values of σ, the curves follow the DebyeHückel result. Deviations from this linear behavior are evident at low x for the four topmost curves. The inset shows the counter- and co-ion distribution for 0.025 Cm^{-2} at 20 mM KCl. The coions are depleted in close proximity to the surface. In contrast, the number density of counterions is ten times higher than in bulk solution.

Far from the surface, the potential decays exponentially with a characteristic length λ for all values of σ. For large enough σ, however, the potential far from the surface no longer increases with increasing σ. Instead, its value becomes independent of the magnitude of σ and takes on the form $\phi(x) = \pm(4k_B T/e)\exp(-x/\lambda)$. Correspondingly, for large enough σ the distribution of counter- and coions far from the surface also becomes independent of the magnitude of σ. In this case all of the additional screening charge is located close to the charged surface, as evidenced by the continued increase of $\phi(x)$ with increasing σ in this region. The size of this region is of the order of the GouyChapman length, λ_{GC}. More precisely, at a planar surface and under conditions of low bulk electrolyte concentration ($\lambda_{GC} \ll \lambda$), half of the counterions reside within λ_{GC} from the surface. In water at room temperature, λ_{GC} is only 0.24 nm for a high surface charge density of σ = 0.16 Cm^{-2} (corresponding to 1 electron per nm^2). Although its value scales inversely with σ, λ_{GC} remains a molecular scale length for many charged systems.

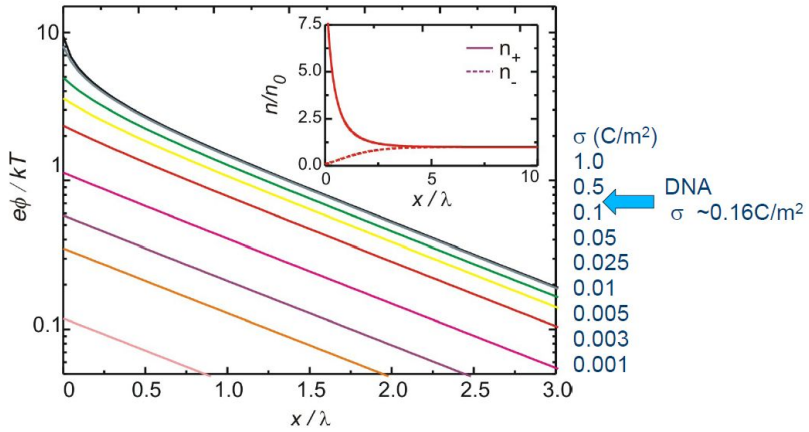

Figure 9.8: Electrostatic potential $\phi(x)$ (in units of k_BT/e) versus position x (in units of λ) as given by the solution to the full PB equation. From bottom to top, the curves correspond to values of the surface charge density s of 0.001, 0.003, 0.005, 0.01, 0.025, 0.05, 0.1, 0.5 and 1.0 C m^{-2} in 20 mM KCl at 300 K. For low values of σ, the curves follow the DebyeHückel result. Deviations from this linear behavior are evident at low x for the four topmost curves. Inset: counter- and coion distribution for $\sigma = -0.025$ C m^{-2} at 20 mM KCl. The coions are depleted in close proximity to the surface. In contrast, the number density of counterions is ten times higher than in bulk solution.

Qualitatively, the charge screening a highly-charged surface can thus be thought of as consisting of two components: a diffuse layer, which extends a few Debye lengths into the solution, and a more compact layer very close to the surface. The diffuse layer is composed of more-or-less symmetric distributions of excess counterions and missing coions, whereas the more compact layer is composed predominantly of counterions. The latter results from the non-linearity inherent in eqn (1): while the coion concentration cannot be suppressed below zero, the degree of counterion enrichment can be arbitrarily high. Even for a surface with $\sigma = 0.025$ Cm^{-2} (corresponding to $e\phi/k_BT \approx 2$) the ion distributions show an excess of counterions n_+ whereas coions n_- are completely depleted in the screening layer.

9.5 DLVO theory

We know have discussed the main forces of interactions that are needed to study one of the main theories used for describing the stability of colloidal suspensions. The main approach describing colloidal particle interactions is the DLVO theory named after Derjaguin, Landau, Verwey and Overbeek. Combining the attraction due to dispersion forces with the repulsion due to electrostatics provides a qualitatively correct total potential interaction between two charged colloids or macro-

molecules. This was accomplished by Deryaguin, Landau, Verwey and Overbeek (DLVO). Note the extremely rich functional form that is obtained by combining eq. 9.11 or eq. 9.7 with Coulomb repulsion, shown in Figure 9.9. There *may* be conditions (high surface charge, low bulk ionic strength, low colloid concentration) under which there is a potential barrier that hinders or prevents aggregation. There may also be a metastable energy minumum at large separations, which is interesting because it corresponds in many systems to the wavelength of light, giving rise to Bragg scattering and (self assembled) "photonic crystals". In its

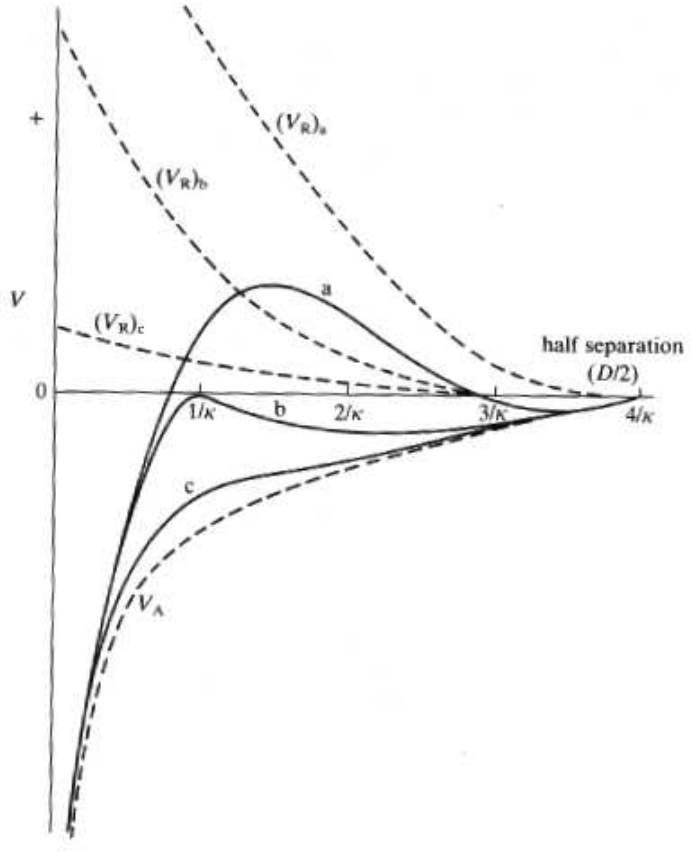

Figure 9.9: Total potential energy of interaction for (a) stable, (b) marginally stable and (c) unstable colloidal suspension. Note that the excluded volume repulsion at distances approaching 0 is not shown on this plot.

functional form DLVO theory is derived by combining the attraction due dispersion forces, U_{vdW} and screened Coulomb repulsion, U_e. The screened Coulomb potential around a spherical particle of radius R and charge Q is given by

$$U_e = \left(\frac{Qe^{\kappa R}}{1+\kappa R}\right)^2 \frac{e^{-\kappa r}}{\epsilon_0 \epsilon_r r} \tag{9.51}$$

with r the distance between the centres of the two interacting particles. U_e is repulsive and used to counteract the attractive dispersion or van der Waals forces given by

$$U_{vdW} = -\frac{\mathcal{B}}{6}\left[\frac{2R^2}{r^2-4R^2} + \frac{2R^2}{r^2} + \ln\left(\frac{r^2-4R^2}{r^2}\right)\right] \tag{9.52}$$

where $\mathcal{B}$ is a constant similar to the discussed Hamaker constant including density and other prefactors. Compared to equation 9.11, equation 9.52 describes the interactions between two spherical particles at finite distance where the surfaces maybe be separated by more than R. We will not discuss the exact derivation in this course. The original calculation can be found in a seminal paper by Hamaker from 1937 and is known as Hamaker summation.

In order to convince ourselves that the form of U_{vdW} agrees with the material in the course so far, we consider the case where the particles (spheres) are very close (result shown in equation 9.11). If we redefine r using the distance h between the surfaces of the spheres we can write $r = 2R + h$. Now in the case of $h \ll R$ we find that U_{vdW} simplifies to

$$U_{vdW} \approx= -\frac{\mathcal{B}}{12}\frac{R}{h} \tag{9.53}$$

which is the expected result. Please note that the decay is even slower than the decay for solid-solid which has h^{-2}. The reason for the slower decay is that even for $h = 0$ attractive forces remain between parts of the spheres that remain further apart. In other words, any change in separation h does not change the distance between other parts of the spheres much, which explains the slower decay of h^{-1} compared to solid-solid with h^{-2}.

Having discussed the more general result for long-range vdW interactions between spheres we can now combine thetwo equations to derive the DLVO result. The full DLVO equation for a pair of spherical particles is obtained by adding U_e and U_{vdW}. The different signs highlight the fact that one is repulsive and the other attractive. Finally, the DLVO potential $U(r)$ can be written as

$$U(r) \approx \left(\frac{Qe^{\kappa R}}{1+\kappa R}\right)^2 \frac{e^{-\kappa r}}{\epsilon_0\epsilon_r r} - \frac{\mathcal{B}}{6}\left[\frac{2R^2}{r^2-4R^2} + \frac{2R^2}{r^2} + \ln\left(\frac{r^2-4R^2}{r^2}\right)\right] \tag{9.54}$$

with some possible solutions shown in Figure 9.9. Depending on the surface charge, the radius and the distance of the colloidal particles one can create barriers that prevent aggregation of the particles creating the barrier as shown by curve a in Figure 9.9. On long time scales and at finite concentrations, aggregation is still most likely as the most stable configuration will be the aggregated state. A good example are gold colloidal (nano-)particles that are coated with molecules rendering the surface strongly (often negatively) charged. These gold-nanoparticle

suspensions can be stable for weeks, months, or even years before demixing will eventually occur.

9.5.1 Other colloidal interactions and stabilisation

So far we have discussed hard core repulsion, Coulomb, and dispersion interactions. They all combined in DLVO. At the start of the chapter we mentioned that there are 5 interactions in total. The two more important interactions in colloid systems will be briefly discussed in the final parts of this chapter. The first we will look at are **steric interactions**. The colloids can be coated with a polymer brush that repels (osmotic pressure of compressing the polymer layer) an approaching similarly coated colloid. The brush can be thick enough to extend into the region where dispersion forces are negligible. The brush itself only induces a negligible dispersion attraction since it is swollen with solvent, i.e. very dilute. A very common example of steric interaction is the $\beta-$casein layer that coats fat globules in milk, keeping these micelles stable.

Depletion interactions are a form of entropic attraction that is at work in any system where there are small components suspended together with the large objects. If the gap between two large colloids becomes smaller than the size of the small colloids (or polymers) there will not be space for the small ones to enter the gap volume. They are depleted from that region. The large colloids are subject to an osmotic force from the small ones from all directions except from within the gap. The result is an effective attraction between the large objects. The range of this interaction is the small object diameter, and the interaction potential is set by the osmotic pressure of the small objects, i.e. usually their concentration. This potential looks like an attractive square well. The square well potential is covered in statistical physics and is one of those potentials for which you can relate the form of the potential to the pair correlation function.

For dilute solutions of polymers or particles (both non-interacting) the osmotic pressure is given by the ideal gas law

$$P_{osm} = \frac{N}{V} k_B T \tag{9.55}$$

where N is the number of polymers in the solution volume V. The interaction potential U_{dep} between the particles is then given by

$$U_{dep} = -P_{osm} V_{dep}. \tag{9.56}$$

The interaction is proportional to V_{dep} which denotes the volume between the particles that excludes the polymers. For two particles with radius a and separation

r one finds that

$$V_{dep} = \frac{4}{3}\pi(a + L^3)\left(1 - \frac{3r}{4(a+L)} + \frac{r^3}{16(a+L)^3}\right) \tag{9.57}$$

where L is the thickness of the depletion layer. The depletion interaction is always attractive and often much weaker than other interactions. The depth of the well is in the range of one k_BT. Increasing the number density enhances the attraction and can lead to phase separation or aggregation in colloidal systems.

9.5.2 Phase diagrams of colloid suspensions

We have introduced 5 types of colloid interactions. The free energy of a colloid system includes these, as well as the configurational entropy of all the components. In a phase transition, some degrees of freedom are affected and some are not. The latter clearly don't affect the transition. Over the last 20 years colloid systems have been a playground for condensed matter physicists because the potential can be tuned almost at will to study various types of transitions.

One of the most important examples are colloid systems where all the interactions except the excluded volume are "switched off". This system is a model for the physics of hard spheres. There is a phase transition from a fluid phase to a crystal. There is also a glass phase (amorphous solid) if the system is compressed "fast". This is still being studied to date. Another important system for physics is the suspension of colloids with depletion attraction. The square well can be tuned in width and depth, mimicking for example the phase diagram of very simple atoms like Argon.

Understanding the interaction potentials and phase transitions in colloids is considered important in finding appropriate general criteria to optimise crystallization. A challenge in molecular biology is to optimise the crystallisation of proteins, in particular membrane proteins, to form crystals large enough for X-ray crystallography. The conditions to form these crystals are currently found empirically, by sampling the huge parameter space (e.g. concentration, pH, temperature, presence of other polymers, salt, solvent...) with modern experimental techniques.

Chapter 10

Electrokinetic Phenomena

10.1 Introduction

Electrokinetic phenomena (EKP) can be loosely defined as all phenomena involving tangential fluid motion adjacent to a charged surface, this can be a stationary surface, charged molecule or particle. Electrokinetic effects are manifestations of the electrical properties of interfaces. We will consider them in this course under steady-state and isothermal conditions. In practice, steady-state measurements are often the only source of information available on that may provide insights into the underlying physical principles. The study of EKP constitutes one of the classical branches of colloid science. Electrokinetics has been developed in close connection with the theories of the electrical double layer (EDL) and of electrostatic surface forces. Hence we will have to study properties of the EDL first.

Especially helpful in the understanding of EKP is the Poisson-Boltzmann (PB) equation. In this part of the course we will discuss the implication of the PB equation for the motion of charged particles and macromolecules in aqueous solutions subject to electric fields.

We will discuss two electrokinetic phenomena driven by electric potentials: electro-osmosis (EO) and electrophoresis (EP). Both EP and EO are created by electric fields that exert opposing forces on the positive and negative charge carriers present in solution. EO and EP are a direct consequence of the motion of these ions transferring momentum to the surrounding liquid and the surfaces. These mechanical forces on ionic charges at the liquid-solid interface are in addition to the direct Coulomb forces acting on the charges on the surface or molecule. As will become apparent in the following discussion, electro-osmosis and -phoresis are intimately related in the thin Debye-layer limit. A third example of EKP will be streaming potentials that are due to pressure driven flows through charged media.

The three examples for EKP will discuss are:

10.1.1 Electrophoresis

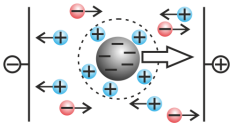

Figure 10.1: Electrophoresis of a negatively charged particle in electric field with counter- and coins .

Electrophoresis (EP) is the movement of charged particles or macromolecules (these are often called polyelectrolyte), under the influence of an external electric field. The main (macroscopic) observables are the electrophoretic velocity, v_e (units ms^{-1}) and electrophoretic mobility, u_e ($\mathrm{m}^2\mathrm{V}^{-1}\mathrm{s}^{-1}$). The latter is defined as $u_e = |v_e|/E$,where E is the electric field strength. The mobility is counted positive if the particles move toward lower potential (negative) electrode and negative when the molecules move towards the positive electrode.

10.1.2 Electro-osmosis

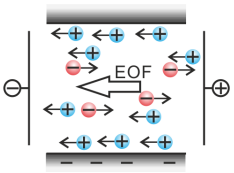

Figure 10.2: Electroosmotic flow in a channel with negatively charged walls due to an applied electric field.

is the motion of a liquid over an *immobilized* charged surface with an electric field applied parallel to it. The motion is the result of the force exerted by the electric field on the movable counter-ions. The counter-ions transfer momentum to the liquid thus giving rise to the electro-osmotic flow. The electro-osmotic flow velocity, v_{eof} (units ms^{-1}), is the uniform velocity of the liquid **far** from the charged interface. Far is in relation to the screening length in the liquid. Other important quantities here are the volume flow rate $Q_{eof,E}$ ($\mathrm{m}^4\mathrm{V}^{-1}\mathrm{s}^{-1}$) divided by electric field strength. Obviously this fluid flow will give rise to an electro-osmotic counter-pressure, Δp_{eof}, which gives the pressure difference that must be applied across the system to stop any volume flow.

10.1.3 Streaming potential

The streaming potential U_{str} and current I_{str} are intimately related to each other. U_{str}, is the potential difference at zero electric current, caused by the flow of liquid over a charged surface. These are usually encountered in fluid flows through charged capillary tubes, micro- or nanofluidic channels. The potential difference is usually measured across the channel. Streaming potentials are due to charge accumulation since the movable counter-ions are displaced by the applied flow. The corresponding streaming current, I_{str} (A), is simply the current when the two sides of the capillary of channel are short-circuited.

In the literature there a number of other phenomena which are closely related but are beyond the scope of this lecture course.

10.2 Charged ions and particles in electric fields

Motion of charges in a field

If there is a gradient in the electrostatic potential, then there will be a force on each charge ze, equal to

$$f_{el} \;=\; zeE \;=\; -ze\left(\frac{\partial\psi}{\partial x}\right) \tag{10.1}$$

The charge will tend to move with a velocity v, and there will be a viscous drag given by $f_{drag} = -\xi v$. At steady state, these two forces will balance, so that $v = f_{el}/\xi$.
As the charges migrate, they accumulate and form a finite concentration gradient $\nabla\phi$. As can be worked out from Fick's law, in the absence of a field this would disappear, the flux of particles is given by: $\mathbf{J} = -D\nabla\phi$. In the presence of an electrostatic field in the x-direction, the total flux of particles will be the sum of both electrostatic flux and diffusion flux, which is $J_{el} = \phi v$:

$$\begin{aligned} J_{tot} &= -D\frac{\partial\phi}{\partial x} - \frac{ze\phi}{\xi}\frac{\partial\psi}{\partial x} \\ &= -\frac{\phi}{\xi}\left[\frac{k_BT}{\phi}\frac{\partial\phi}{\partial x} + ze\frac{\partial\psi}{\partial x}\right] \\ &= -\frac{\phi}{\xi}\frac{\partial\mu'}{\partial x}, \end{aligned} \tag{10.2}$$

where the chemical potential μ' is given by:

$$\mu' \;=\; \mu^0 \;+ k_BT\ln\phi(x) \;+\; ze\psi(x). \tag{10.3}$$

Note how the chemical potential of the dilute system is modified by the presence of the field. At equilibrium, the chemical potential gradient is zero, and the flux of particles driven by the electrostatic field is balanced by the diffusion flux.

10.2.1 Electro-osmotic flow between parallel plates

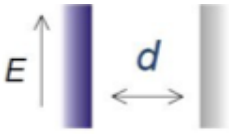

Figure 10.3: Parallel plates one charged with electric field applied along the surface.

We now consider two parallel plates with low surface charge as introduced in Figure 10.3. Since we require electroneutrality for the system the surface charge leads to more counterions than co-ions in the gap. For channels of finite length the abundance of counterions leads to a voltage drop at the entrances of the channel. This potential difference is also known as Donnan potential and is a common

feature of channels especially in biological systems. The Donnan potential in the channel V_D is given by

$$V_D = \frac{k_B T}{2e} \log \left[\frac{n_+}{n_-} \right] . \tag{10.4}$$

The ratio of counter- to co-ions determines the potential. Higher charge of the channel walls leads to a higher V_D in the channel and hence also signals a greater difference between the movable counter-ions that screen the wall charges (Figure 10.2) and the co-ions. With an applied electric fields the counter-ions start to move and transfer more momentum onto the solvent molecules than the co-ions. The imbalance of the momentum leads to a solvent flow. For negative charged walls the positive counter ions are moving to the negative electrodes and hence the electro-osmotic flow goes from right to left (Figure 10.2). We will now calculate the electro osomotic flow between parallel plates where one is charged and one is uncharged.

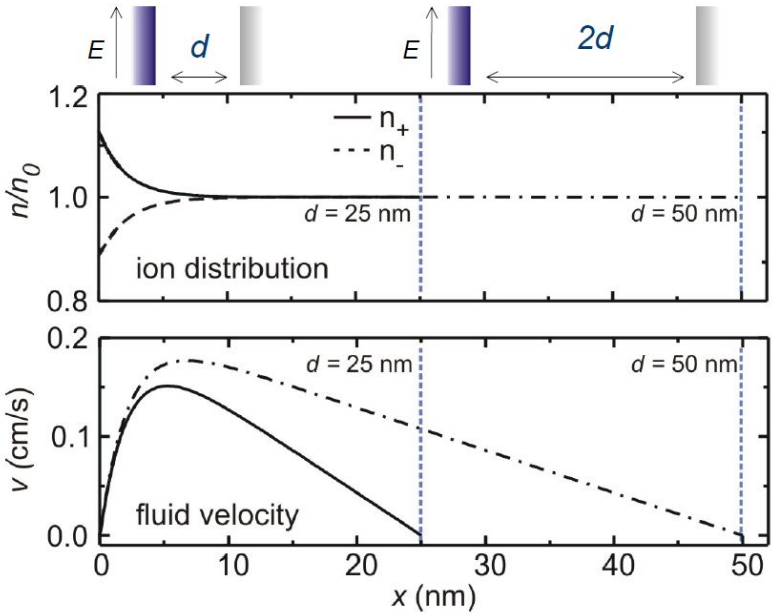

Figure 10.4: Parallel plates with on charged plate and one uncharged. The ion distribution for low surface charge of co- and counter-ions is shown as a function of distance of the plates. The distance of the plates does not change the ion distribution. The fluid velocity due to an EOF is shown in the lower graph. Here the distance between the plates makes a difference as, in contrast to the screened Coulomb interactions, the hydrodynamic interactions extend from one surface to the other. Despite the same surface charge the maximum flow velocity as well as the total flow are high for the larger plate distance of $2d$.

We now apply an electric field along the gap, parallel to the planes and want to calculate the EOF due to the mismatched charges in the screening layer.Before we

start we can make further simplifications. We are interested in describing flows at length scales that are typical for biological or other sift systems, i.e. length scales of microns or less. At these length scales, with the typical viscosity of water and considering the typical velocities of mm/s encountered in electroosmotic flows, the Reynolds number remains very small and all flows can expected to be laminar. Furthermore, from symmetry the fluid velocity can only be oriented parallel to the electric field (z-direction) and can only vary perpendicular to the surface (x-direction). Under these conditions the Navier-Stokes equations that describe fluid motion reduce to the simple form

$$\frac{d^2 v_{eof}}{dx^2} + \frac{\rho(x)E}{\eta} = 0 \tag{10.5}$$

where $\rho(x)E$ is the force per unit volume exerted by the electric field.

The ion distributions for a surface with low charge is shown in Figure 10.4. Due to the low charge the distributions of counter-ions and co-ions are completely symmetric. In the EDL hence are both co- and counter-ions present (Figure 10.4). The electric field applied along the surface will now move the ions in the liquid and hence transfer momentum to the fluid and set up an EOF.

Using $\rho(x)$ this simplified Navier-Stokes equation can be directly integrated

$$v_{eof} = \frac{E\sigma\lambda}{\eta} e^{-x/\lambda} + Bx + C. \tag{10.6}$$

With the usual no-slip boundary conditions at the two walls $v_{eof}(0) = v_{eof}(d) = 0$ the flow profile is

$$v_{eof} = -\frac{E\sigma\lambda}{\eta}\left(1 - e^{-x/\lambda} - \frac{x}{d}\right). \tag{10.7}$$

This result is shown in Figure 10.4 together with the distribution of ionic species for walls separated by $d = 25$ nm and $d = 50$ nm, respectively. Note that the the charge densities of co- and counter-ions are unchanged but the flow field is changing with larger maximum velocity and overall larger flow.

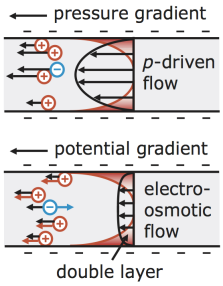

Figure 10.5: Comparison of streaming potential (top) and EOF (below). Notice the difference in the flow profiles.

10.2.2 Streaming currents and potentials

This part of the chapter was inspired and guided by discussions with Lyderic Bocquet and Derek Stein who also kindly shared material.

We looked at EOF that was the response of the system to an applied electric field. In all fluidic channels fluids, electric charges and heat can be driven by gradients set up by externally controlled parameters like pressure, voltage and temperature. For small $\nabla\phi_j$ of the respective potentials ϕ_j the resulting diffusive

currents are given by

$$J_i = \sum_j L_{i,j} \nabla \phi_j \tag{10.8}$$

where $L_{i,j}$ represents a matrix detailing each relationship between gradient and current. Onsager showed that $L_{i,j}$ must be symmetric. EOF is an excellent example to illustrate the symmetry.

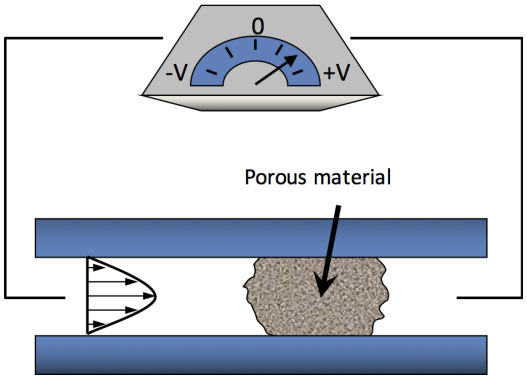

Figure 10.6: Schematic of the system used by G. H. Quincke in 1859 to measure streaming potetntial for the first time. The system also confirms the reciprocity between mechanical motion and electric flow.

As electric fields applied along parallel plates gives rise to EOF, Consequently, an applied pressure gradient should lead to a 'streaming' potential and associated current as illustrated in Figure 10.5. In other words, forcing salt solutions through confined channels with a finite surface charge should lead to charge separation and hence a current and electric energy. This is known as streaming potential and was first described by Quincke in 1859. In his experiment, as shown in the schematic Figure 10.6, he pushed salt water through a porous material and measured a resulting voltage due to the build up of one counter ions in one of the reservoirs.

For a geometry with two identical plates one can model the streaming current I_{str} to the product of the charge density, $\rho(x)$, and the local speed of the fluid, $v(x)$, integrated over the cross section of the channel

$$I_{str} = w \int_{h/2}^{h/2} \rho(x) v(x) dx \tag{10.9}$$

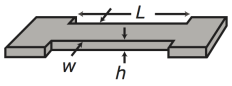

Figure 10.7: Schematic of the channel for streaming current measurements. Please note that $L \gg h, w$.

where x i s the height from the channel mid-plane and w is the channel width, Figure 10.7. We ignore sidewall effects because $w \gg h$, and treat the flow and charge density profiles as uniform over the width of the channel, as in an infinite parallel-plate geometry. The velocity distribution is described by a Poiseuille flow subject

to the no-slip boundary condition at the walls: $u(x) = -\Delta P(h^2 - 4x^2)/8\pi L\eta$, where L is the length of the channel, ΔP the pressure difference, and η the fluid viscosity.

The streaming current should increase linearly with the applied pressure and this is observed in wide glass nanochannels that closely resemble the plan parallel plate configuration as discussed. A typical experimental setup with a schematic is shown in Figure 10.8.

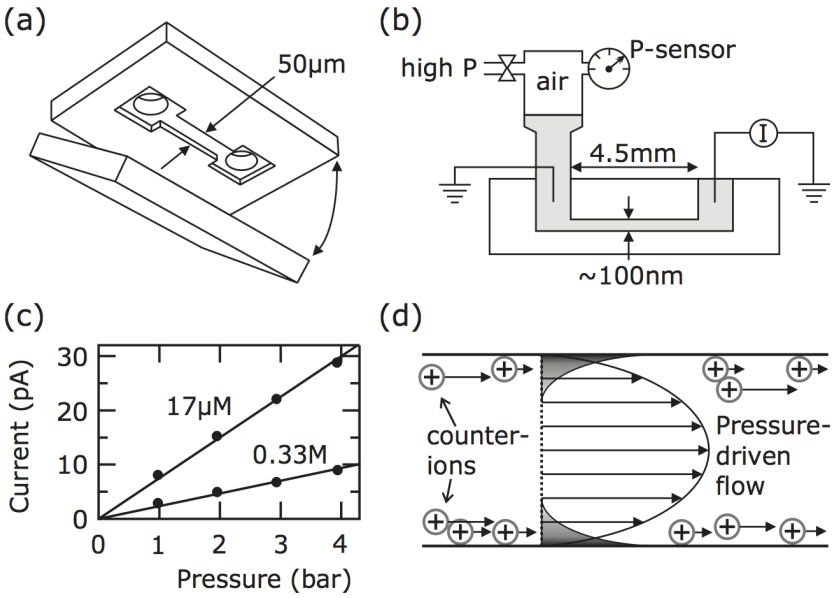

Figure 10.8: (a) Nanochannels are fabricated by covalently bonding two pieces of fused silica. The top piece contains an etched nanochannel and two 1 micron diameter holes for the fluid connections. (b) Schematic side view of the nanochannel - not to scale. The length of the channel is much larger than width and height. (c) Streaming current as function of pressure for a typical 140 nm high channel at low and high salt concentrations. Lines are linear fits to the data. (d) Schematic illustration of the origin of the streaming current due to the mismatch of movable charges in the electric double layer screening the charges on the silica surfaces.

10.2.3 Efficiency of energy production

There are efforts to develop this technology into a viable alternative to create energy. However, the reported efficiencies are still low and reach only a few percent in ideal situations. The main reason is the large flow resistance of small hydrophilic channels due to the no-slip boundary condition on the surface. However, hydrophobic materials like carbon nanotubes or channels coated with graphene layers may decrease the flow resistance, increase the velocity and hence lead to

enhanced efficiencies. There are several companies that are working on commercial systems to create 'blue' energy.

10.3 Electrophoresis

10.3.1 Helmholtz-Smoluchowski equation

The introduction of the EDL and the ζ-potential allows us now to set up a simple model for systems with thin Debye layers, i.e. when the ζ-potential can be used. We will compare the results from an experiment of a single, charged, mesoscopic particle with the theory. In order to distinguish the treatment of ions and particles and emphasize that the observables can be directly connected to experimental parameters we will us a different notation than in equation 10.1. The experiment looks at one spatial parameter $x(t)$ and hence we use d instead of ∂. Consequently we use the applied voltage $V(x)$ instead of the potential $\psi(x)$.

We start to model electrophoretic motion of a colloidal particle with charge ze in solution by calculating the force in an electric field E as

$$F_{ep} = -ze\frac{dV(x)}{dx} = zeE, \tag{10.10}$$

where $V(x)$ is the electric potential. For simplicity we assume a uniform electric field E =constant which can be achieved by designing a suitable experimental geometry. However since we are in liquid we have to consider the Stokes friction on the moving particle γv_e into account and thus in steady state we have

$$F_{ep} - v_{ep}\gamma = 0. \tag{10.11}$$

Since the diffusion current $J_e = cv_e$ we can write down the concentration of particles c along the field

$$J_{ep} = -\frac{zec}{\gamma}\frac{dV}{dx}. \tag{10.12}$$

Remember that $1/\gamma$ is the mobility of the particle.

In order to extract the surface potential ζ of the particle we need to replace ze in the last equation. It can be noted that $\epsilon_r\epsilon_0\zeta\gamma/\eta$ has the units of a charge. Here we assume that the diameter of the particle is much larger than the Debye screening layer which is a reasonable assumption for many experimental situations. Following this major simplification we have

$$J_{ep} = -\frac{\epsilon_r\epsilon_0\gamma\zeta c}{\gamma\eta}\frac{dV}{dx}. \tag{10.13}$$

It directly follows for the electrophoretic velocity v_e

$$v_{ep} = -\frac{\epsilon_r \epsilon_0 \zeta}{\eta} \frac{\partial V}{\partial x} = \frac{\epsilon_r \epsilon_0 \zeta}{\eta} E \tag{10.14}$$

and the Helmholtz-Smoluchowski equation for the mobility u_e

$$u_{ep} = \frac{\epsilon_r \epsilon_0 \zeta}{\eta}. \tag{10.15}$$

This is valid when we introduce the ζ-potential and hence ignore any details about the particle. If the particle has positive charge, its ζ-potential is positive and negative of the surface charge is negative.

The ζ-potential depends on both the experimental parameters of the measurements. The reason for the dependence of the ζ-potential on other details is due to the major assumptions that are needed to describe the surface properties with a simple potential. It is important to stress again the key assumption: the diameter of the particle is much larger than the screening length. In other words, the Helmholtz-Smoluchowski description in equation 10.15 is valid if the typical radius a of a charged particle or molecule is much larger than the Debye screening length. The Debye screening length in an aqueous electrolyte solution with monovalent ions of 0.1M concentration is $\lambda \approx 1$ nm at room temperature. If $\lambda \ll a$ we can ignore the details of the double layer structure that we discuss later in more detail. It is important to note here that the sign of the mobility depends on the definition of the coordinate system with respect to the direction of the electric field.

10.3.2 Limitations

As the concept of ζ-potential this is also a simplified approach which neglects several important phenomena:
(i) it does not include the treatment of strongly curved surfaces (i.e., surfaces for which the condition for the screening length does not apply);
(ii) surface conduction in the diffuse layer and closer to the surface is not taken into account
(iii) polarization of the electric double layer is not taken into account, i.e. charged dipoles and other higher order effects like dielectrophoresis are not captured in this formalism.

However, checking the validity of (i) is straightforward, (ii) will be briefly discussed later and is often only relevant when $\zeta > 50$ mV. Polarization would account for the accumulation of charge in front and back of the moving particle which would result in a dipole moment and thus an additional field.

10.3.3 Testing Helmholtz-Smoluchowski using single colloid electrophoresis

We will now demonstrate with a single particle electrophoresis that the Helmholtz-Smoluchowski description works for large particles. One experimental system which allows for testing the ζ-potential concept is a single colloid trapped in the focus of an optical trap[1] The Setup with the particle in an optical trap is shown in Figure 10.9. Assuming that the electrical field is constant and just a function of time we can easily measure electrophoretic mobility $u_e = v_e/E$ of the particle. Since we work with an optical trap we also have the optical tweezers restoring force $F = -\kappa\Delta x$ thus we get for the effective speed v_{eff} of the colloid in the optical trap

$$v_{eff}(t) = -\frac{\kappa\Delta x(t)}{6\pi\eta r} + u_e E(t) \tag{10.16}$$

where $\Delta x(t)$ is the time dependent excursion of the colloidal particle from the optical trap center. If $E(t)$ oscillates with frequency f, the average velocity over

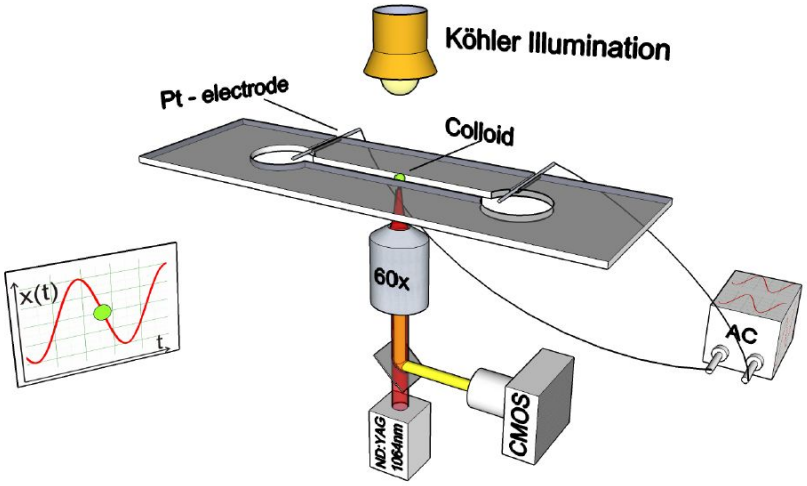

Figure 10.9: Optical tweezers for testing Helmholtz Smoluchowski equation in a single colloidal particle in a slowly oscillating AC field. The velocity of the particle is measured as it the force on the particle.

a full period is $v_{eff} = 4\Delta X f$. ΔX is the maximum amplitude of the oscillation. It follows

$$v_{eff} = 4\Delta x f = -\frac{\kappa\Delta x(t)}{6\pi\eta r} + u_e E \tag{10.17}$$

[1]Optical tweezers trap particles in a focussed laser beam. The 3 dimensional trap sets up a harmonic trap that allows for force measurements like with a Hooke spring: $F = -\kappa\Delta x$ where κ is the stiffness of the optical trap and Δx the distance of the particle from the trap centre.

and thus we get

$$|u_e| = \frac{4\Delta X f}{E} + \frac{\kappa \Delta X}{6\pi\eta r E} \tag{10.18}$$

and $\Delta X/E$ can be simply extracted from the data. Assuming that we can use the ζ-potential which is true for frequencies of a few 100 Hz and lower we get

$$\zeta = \frac{\eta}{\epsilon_r \epsilon_0} u_e. \tag{10.19}$$

Typical experimental data on colloids with radius $r = 1.11$ μm in 1 mM KCl at pH=8 at $f = 80$ Hz is shown in $Figure$ 10.10. The electrophoretic mobility is extracted from the gradient of the fit to the experimental data. This measurements is performed on a single colloidal particle in an optical trap and hence allows for testing the Helmholtz-Smoluchowski equation. From the measurements one extracts a constant ζ-potential of 33 mV for the particle. Remember that these experiments are done at low Reynolds number and hence the system is at each time in equilibrium, which means that the electric force and the friction cancel each other. Hence the force is a directly proportional to the electrophoretic velocity v_e. These experiments are performed at a distance of around 50 micron from any surface.

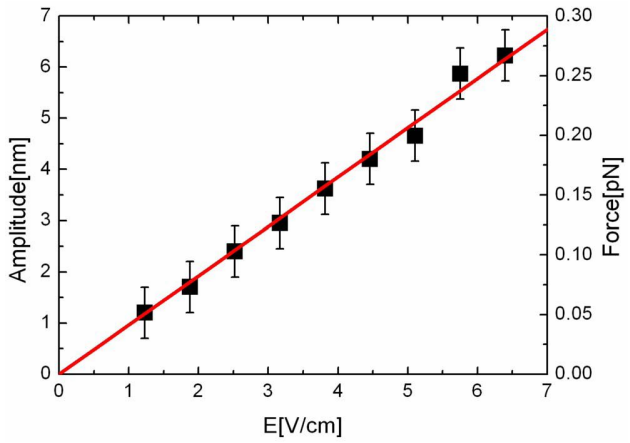

Figure 10.10: Amplitude and force on a charged particle in a uniform electric field E as measured by optical tweezers. The linear dependence of the force on the electric field shows that the particle can be described with a constant ζ-potential.

10.4 Zeta-potential and atomic details of double-layer

At this point it is worth to discuss the reason to use the zeta-potential. Until now we just looked at the diffuse part of the double-layer without considering any

atomic details of the surface and ions. While the PB equation is very successful to capture many of the basic principles, in systems with EOF simultaneous solutions of the Navier-Stokes equation are necessary. This brings about a very rich behavior with many counter-intuitive results that we will not discuss here. In addition there is the problem of the finite size of ions. The screening length can easily approach of around or even less than 0.3 nm in salt concentrations of $\geq$1M KCl. Even at physiological conditions with an ionic strength of about 150 mM we have to work with a screening length of roughly 1 nm. At these length scales the screening length approaches the diameter of the ions with their water shell. The diameter of a water molecule is about 0.2 nm which is also on the order of λ. For a full description of EKP at high salt concentrations the finite size of water and counterions will have to be taken into account. However this is beyond the scope of this lecture.

One common approach to keep the interpretation of real systems simple a new parameter is introduced which has achieved wide-spread acceptance. This is the zeta-potential which combines a number of assumptions and works quite well for a set of well-defined experimental conditions. The definition is best explained by considering a more detailed image of the electric double layer on charged surfaces in liquids as shown below in Figure 10.11.

The ζ-potential denotes the potential at the no-slip plane at distance d^{ek} from the surface with surface charge σ^0 and surface potential Φ^0. The zeta(ζ)-potential is always smaller than the bare surface potential and is defined through a number of assumptions:

- there is a thin layer that does not contain any charges due to an absorbed water layer etc. Thus at the inner Helmholtz plane (IHP) we have potential $\Phi^i < \Phi^0$
- the surface will have a certain potential Φ^0 but this will be reduced by adsorbed (fixed) ions in the outer Helmholtz plane (OHP) with $\Phi^d < \Phi^i$
- these ions are fixed and have another charge free layer thus $\zeta < \Phi^d$ which can be significantly smaller than Φ^0 this defines also the no-slip plane
- shear is generated only at the slip plane since only there water and ions can start moving

The IHP and OHP are often referred to as Stern layer. The Stern layer does not distinguish between the IHP and OHP encompassing everything close to the surface below the no-slip plane.

It is important to emphasize here that the exact position of the slip plane is not known. ζ is also depending on the type and valency of the counter-ions, the salt

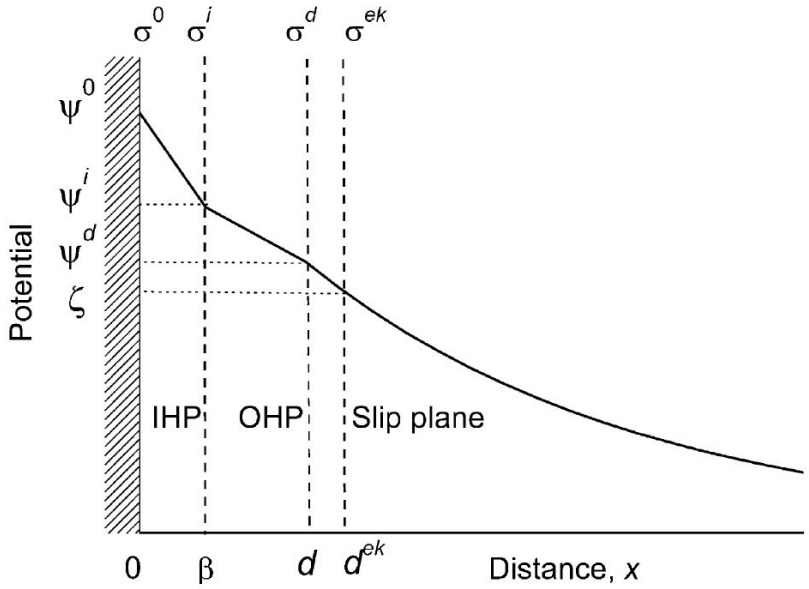

Figure 10.11: Detailed view of the double layer close to the surface. The bare surface has potential Ψ at $x = 0$. The first plane (or layer) is called the inner Helmholtz plane (IHP) and contains counter ions and water. The potential is reduced at the end of this layer to Ψ^i. Then follows the outer Helmholtz plane (OHP) that further reduces the surface potential to Ψ^d. OHP and IHP are also together known as Stern layer. The slip plane starts at distance d^{ek} from the surface and the potential on that plane is the ζ-potential.

concentrations and the geometry of the system complicating the situation. Since ζ is defined by being the potential where water and ions start freely moving it is a very successful parameter for describing electro-kinetic behaviour of a system in a well defined set of conditions. Thus ζ is a parameter that depends on the details of the measurements and often even on the method as it depends on the specific details of the model used to extract it from the experimental data. However, as the bare charge of the surface is usually impossible or hard to measure and may also depend on the pH of the solution the ζ-potential it is still in wide-spread use in the field of colloidal science.

10.4.1 Double-layer capacitance

The electric double layer has a complicated structure beyond the no-slip plane, however, there are experiments that can probe the IHP and OHP. Most hydrophilic surfaces carry some kind of charge in aqueous solution. Considering the split charges in the double layer, the extend of the EDL should be measurable by making a capacitance measurement. The EDL can be regarded as a capacitor. The EDL capacitance is essential for the transport of charges in salt solutions/electrochemical

cells like batteries and fuel cells and exists on any biased metal surface.

Measuring the the differential capacitance yields information about rearrangements in the inner and outer Helmholtz planes and the experimental relevant time scales. Since this technique is widespread we show an example result of a measurement in **??**.

The thickness of IHP and OHP one can investigate through a measurement of the differential capacitance C_{diff} at high salt concentrations where the Debye screening length is shorter or at least similar

$$C_{diff} = \frac{dQ}{dV} \tag{10.20}$$

with Q as the charge on the capacitor and V the applied AC voltage. With $I_C = dQ/dt$ we get

$$I_C = \frac{dQ}{dV}\frac{dV}{dt} = C_{diff}\frac{dV}{dt}. \tag{10.21}$$

To get an impression about the order of magnitude we can estimate the capac-

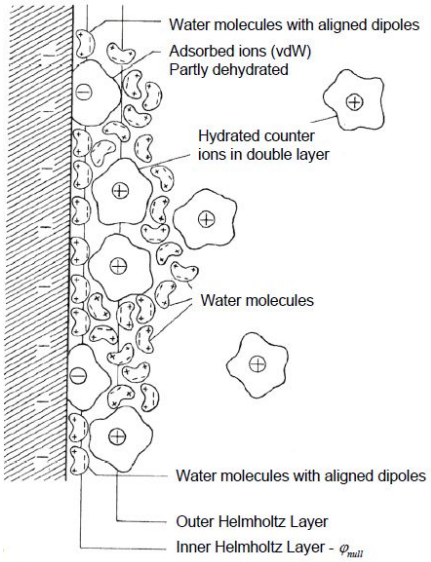

Figure 10.12: Schematic of the EDL with IHP and OHP shown with counter ions and absorbed co-ions on an ideal metal electrode with negative potential.

itance. In strong aqueous electrolytes and assuming that the double layer is a parallel plate capacitor, the capacitance per unit area is $C/A = \epsilon_0\epsilon_r/d$. With d around 0.2 nm - the thickness of the IHP - we get $C/A \approx 350$ μFcm^{-2}. This is an overestimation by a factor of 7 compared to the measured values of 5-50 μFcm^{-2}. This discrepancy is due to the reduced ϵ of water on the electrode surface. In the Stern layer one finds that ϵ can be as low as 6. More than order of magnitude

lower than $\epsilon = 80$ of free water. ϵ_r is reduced since the polar water molecules are fixed near the surface as rotational degrees of freedom are reduced (Figure 10.12).

At high salt concentration and short Debye screening length, the system can be described by two capacitors in series. One is set up through the dipoles of the water and the second by the charges in the IHP and OHP. ϵ is also not constant but a function of distance from the surface. So the capacitance of the Stern layer C_{Stern} is

$$\frac{1}{C_{Stern}} = \frac{1}{C_{dipole}} + \frac{1}{C_{IHP-OHP}} \approx \frac{a_{H2O}}{\epsilon_{dipole}} + \frac{a/2}{\epsilon_{IHP}} \tag{10.22}$$

where a_{H2O} is the diameter of water and $a/2$ is the radius of the hydrated counter ions. This is valid for short screening length below 1 nm when the Debye screening length is within or close to the IHP and OHP. It is important to note here that Figure 10.11 shows the case for low concentration and thus Debye length much larger than IHP and OHP. The molecular details as shown in Figure 10.12 assume high concentration and hence Debye similar or shorter than IHP and OHP.

In the case of Figure 10.11, when the Debye screening layer extends beyond the Helmholtz planes, there is an additional capacitance that needs to be taken into account due to the extend of the Debye screening layer. For small salt concentrations the presence of the diffuse layer beyond the IHP and OHP has to be taken into account by adding a third term to equation 10.22. In the example data, the reduction in capacitance is directly apparent as shown in **??** at low ionic strengths (0.01 mol/L and 0.001 mol/L). The reduction in capacitance indicated by the arrows in **??** originates from the fact that at low concentrations the Debye screening layer reaches beyond the thickness of the IHP and OHP. The capacitance in the low salt case now requires a third, dominating term in equation 10.22 as the screening length is much larger than the molecular length scale of IHP and OHP.

The details of the electrochemical measurements of the capacitance and its application go beyond this course and can be found in any electrochemistry textbook. However, it is interesting to note that upon application of a few 100 mV and given the thickness of less than a nm the field strength in the Stern layer can easily reach 10^8 V/m. This is enough to alter the stability of weak molecular bonds near the electrode surface and lead to the dissociation of weak acids. It is also possible to build ionic transistors and diodes by using the presence of the double layer and either a fixed surface charge or with electrode materials. These systems are under active development at the moment as they could be used for desalting solutions or the control of molecular flow.

10.5 Applications

10.5.1 Electrophoretic separation of DNA molecules

The separation of DNA molecules by gel electrophoresis the process of driving the molecules through a dense network of cross-linked polymer with an applied electric fieldcounts among the most important techniques in biochemistry and molecular biology. Despite the importance of the applications of DNA electrophoresis, however, the fundamental underlying mechanisms responsible for separation have not been fully elucidated, and doing so represents a substantial challenge. Conceptually, it requires understanding the interplay between polymer dynamics, electroosmosis, the topology of the gel and, in many cases, specific interactions between the DNA and the gel matrix. Experimentally, elucidating the role of these different contributions requires probing at or near the molecular scale. In addition to the fundamental interest from the point of view of polymer science and soft matter physics, present attempts to better understand electrophoresis are motivated by our increasing ability to construct sophisticated fluidic systems for manipulating DNA and other macromolecules. Such understanding may provide the insight necessary for developing new separation methods capable of outperforming the traditional gel.

Because of its emphasis on quantitative understanding, the contemporary literature on DNA electrophoresis may be difficult to access for researchers from outside the field. In particular, it is often difficult to separate the well-understood basic ideas from further refinements and details aimed at improving quantitative accuracy. It is the aim of this section of the course to introduce some of the basic ideas while concentrating on conceptual understanding rather than quantitative accuracy of gel electrophoresis.

10.5.2 Gel electrophoresis

Gel electrophoresis is one of the most important separation techniques for long charged macromolecules. As you will show in one of the problem sheets, long DNA molecules are behaving as 'free-draining' coils if they are long enough (longer than $\sim$400 bp). Polymer coils are described as free draining if solvent molecules are able to flow past each segment. A free draining polymer coil in an electric field is not behaving as a colloidal particle of equivalent size and hence be described as a solid particle with a radius given by the radius of gyration. In other words, long polymer coils that have the same charge per segment are described by a ζ-potential and thus the mobility is independent of their length. Separation by length of free-draining polymer coils is not possible.

However, separation can be achieved by letting the polymer migrate in a gel

matrix containing a mesh of polymers. Obviously the interactions between the electrophoretically driven DNA and the mesh will depend on the length of the molecule. Gel electrophoresis was the basis for most sequencing techniques until 10 years ago and was used for the Human Genome Project. Recent advances in sequencing technology have replaced gel electrophoresis as a tool for ultra-fast sequencing but the technique is still of major importance for the separation of macromolecules by length, mass and ζ-potential.

In order to produce a gel one can use molecules extracted from cell walls of *agarophyte* red algae. The agarose monomer and a typical mesh (SEM image) is shown in Figure 10.13 The agarose polymerizes into long fibres that effectively

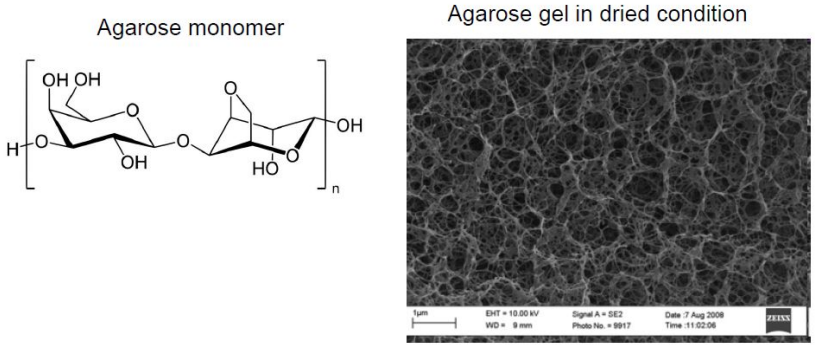

Figure 10.13: The monomer of the agarose gel that forms the fibres after heating and cooling down as shown in the SEM image on the right. Interactions between the DNA molecules and the gel fibres are steric in nature only.

create a network of pores. This system is very similar to concentrated polymer solutions. The DNA moves through this gel by driven diffusion due to an applied electric field. The mobility of the polyelectrolyte is controlled by the effective pore diameters. It is easy to adjust the mobility as the pore diameters in the gel are controlled by the density of agarose in the water when the gel is formed. Increased density leads to smaller pores. For single stranded DNA or small proteins other gel forming systems can be used as well like polyacrylamide (PMMA).

Polymer dynamics - Rouse model

In the simplest approach to describe the molecular dynamics of a polymer chain, we assume that a long polymer is described as a string of N beads. The beads are connected by springs and from a freely jointed chain. Importantly, the monomers can move through each other, so there are no excluded volume effects. Each bead in the chain has a friction coefficient β that is independent on the position within or the shape of the chain. In addition we assume that the chain is free-draining,

there are no hydrodynamic interactions between the beads. These assumptions are known as the Rouse model. The diffusion coefficient in the Rouse model of the polymer is just $D_R = k_b T/N\beta$. The time it takes the chain to diffuse along its end-to-end distance $R_N \approx bN^\nu$ is known as the Rouse time τ_R. For an ideal chain we get

$$\tau_R \approx \frac{R_N^2}{D_R} \approx \frac{R_N^2}{k_B T/N\beta} = \frac{\beta}{k_B T} N R_N^2. \tag{10.23}$$

For an ideal chain $\nu = 1/2$ and hence we get

$$\tau_R \approx \frac{\beta b^2}{k_B T} N^2. \tag{10.24}$$

where b is the size of the monomer bead. Within the Rouse model, one can link τ_R to the characteristic time τ_0 for a monomer to diffuse over its own length if it is not linked to the chain. τ_0 is approximated by

$$\tau_0 \approx \frac{\beta b^2}{k_B T}, \tag{10.25}$$

Here, $\beta \approx \eta r$ is the friction coefficient of the monomers in the chain. With the definition of τ_0 we can now rewrite τ_R and find that

$$\tau_R \approx N^2 \tau_0. \tag{10.26}$$

The Rouse model predicts that the diffusion time as τ_R is proportional to the square of the number of monomers N. If we assume that β is linked to the viscosity of the solution η as $\beta \approx \eta b$ we can rewrite the Rouse monomer time τ_0 and the chain relaxation time as

$$\tau_0 \approx \frac{\eta b^3}{k_B T} \text{and} \tau_R \approx \frac{\eta b^3}{k_B T} N^2. \tag{10.27}$$

When probed on time scales smaller than τ_0, the polymer chain appears static and will respond elastically. For time scales much larger that τ_R one recovers diffusion. On intermediate timescales the chain behaves viscoelastically and the scaling exponents are smaller than 1.

There are obvious problems with this model since we assumed an ideal chain, unrealistic hydrodynamics (beads are independent) and there are no knots. A more realistic approach is to take into account the hydrodynamic interactions by defining a no-slip boundary condition on the chain and remove the free draining aspect. With the inclusion of a no-slip boundary condition, we get the Zimm model. Here, $\beta \approx \eta r$ is the friction coefficient of the monomers and thus the Zimm diffusion coefficient D_Z is

$$D_Z = \frac{k_B T}{\eta R} \approx \frac{k_B T}{\eta b N^\nu} \tag{10.28}$$

R is the radius of gyration of the polymer chain, and ν is the Flory-exponent which is depending on the chain characteristic. For $\nu = 0.5$ we have an ideal chain while with $\nu = 0.588 \approx 3/5$ we can describe a self-avoiding chain.

The Zimm relaxation time τ_Z is then

$$\tau_Z \approx \frac{R^2}{D_Z} \approx \frac{\eta}{k_B T} R^3 \approx \frac{\eta b^3}{k_B T} N^{3\nu} \approx \tau_0 N^{3\nu}. \tag{10.29}$$

The main difference to the Rouse time is the slightly weaker N dependence of the τ_Z compared to τ_R.

The polymer dynamics can also be broken down into sub-chains which behave in the same way as the entire chain. There are N modes of the chain depending of the number of monomers $p = 1, 2, ..., N$ we get

$$\tau_p = \tau_0 \left(\frac{N}{p} \right)^2. \tag{10.30}$$

One can then get the mean square displacement of a segment with p monomers

$$< |\vec{r}_j(t) - \vec{r}_j(0)|^2 > \approx b^2 \frac{N}{p} \approx b^2 \left(\frac{\tau_p}{\tau_0} \right)^{1/2} \tag{10.31}$$

which is directly related to the relaxation time τ_p of the relaxation modes. Interestingly, this results is the same as for monomer diffusion at times below the Rouse time ($\tau_0 < t < \tau_R$)

$$< |\vec{r}_j(t) - \vec{r}_j(0)|^2 > \approx b^2 \left(\frac{\tau_p}{\tau_0} \right)^{1/2}. \tag{10.32}$$

The monomer diffusion is slowed down in the chain. For free Fickian diffusion of a monomer one would get

$$< |\vec{r}(t) - \vec{r}(0)|^2 >= 6Dt. \tag{10.33}$$

Thus in the Rouse regime the mean-square displacement is sub-diffusive as for the Zimm modes which by following the same arguments is given by

$$< |\vec{r}_j(t) - \vec{r}_j(0)|^2 > \approx b^2 \left(\frac{\tau_p}{\tau_0} \right)^{2/3} \text{ for } \tau_0 < t < \tau_Z. \tag{10.34}$$

Reptation

In a gel the Zimm and Rouse models have to be modified since the chain segments cannot move independently from one another. This is very similar to the situation

to a polymer melt of entangled chains which can overlap and cannot cross each other. For polymer melts Edwards developed the reptation model which assumes that the chain is moving in a tube defined by the surrounding chains. The tube diameter r_t is given by $r_t \approx b\sqrt{N_e}$ where N_e is the averaged number of monomers between two entanglements. r_t is also known as the entanglement length. Moving from the concept of monomers to a more coarse grained interpretation of the chain one can define the extension of the Edwards tube R_0 as

$$R_0 \approx r_t\sqrt{N}N_e \approx b\sqrt{N}. \tag{10.35}$$

One can also define a coarse grained contour length of the chain that is closely related to r_t and N_e

$$< L > \approx r_t \frac{N}{N_e} \approx \frac{b^2 N}{r_t} \approx \frac{bN}{\sqrt{N_e}}. \tag{10.36}$$

The diffusive motion in this tube is called reptation and the diffusion coefficient is the Rouse diffusion coefficient $D_c = k_B T/N\beta$. With this we can define the reptation time τ_{rep} for the chain to diffuse out of its tube of length $< L >$

$$\tau_{rep} \approx \frac{< L >}{D_c} \approx \frac{\beta b^2}{k_B T}\frac{N^3}{N_e} = \frac{\beta b^2}{k_B T} N_e^2 \left(\frac{N}{N_e}\right)^3 \tag{10.37}$$

with the lower limit for the reptation time for $N = N_e$

$$\tau_e \approx \frac{\beta b^2}{k_B T} N_e^2 \tag{10.38}$$

and thus

$$\frac{\tau_{rep}}{\tau_e} \approx \left(\frac{N}{N_e}\right)^3. \tag{10.39}$$

Now we can write down the mean-square displacements of the entangled case in the same way as in the free Rouse case. At $t < \tau_e$ this is the motion of the monomers:

$$< |\vec{r}_j(t) - \vec{r}_j(0)|^2 > \approx b^2 \left(\frac{t}{\tau_0}\right)^{1/2}. \tag{10.40}$$

At time $\tau_e < t < \tau_R$ the motion is confined by the reptation tube and thus we get a new coordinate $\vec{s}_j$ along the tube

$$< |\vec{s}_j(t) - \vec{s}_j(0)|^2 > \approx b^2 \left(\frac{t}{\tau_0}\right)^{1/2} \approx r_t^2 \left(\frac{t}{\tau_e}\right)^{1/2} \tag{10.41}$$

related to the reptaion tube diameter r_t. The reptation tube itself is a random walk with step length r_t

$$< |\vec{r}(t) - \vec{r}(0)|^2 > \approx r_t \sqrt{< |\vec{s}_j(t) - \vec{s}_j(0)|^2 >} \approx r_t^2 \left(\frac{t}{\tau_e}\right)^{1/4} \tag{10.42}$$

which is even slower than the unrestricted Rouse motion, as expected in entanglement. Finally we for times longer than the rouse time $\tau_R < t < \tau_{rep}$ the whole chain is moving and thus all segments are correlated. Thus the whole chain diffuses in the reptation tube with the curvilinear diffusion coefficient D_c

$$< |\vec{s}(t) - \vec{s}(t)|^2 > \approx D_c t \approx b^2 N \frac{t}{\tau_R} \approx r_t^2 \frac{N}{N_e} \frac{t}{\tau_R} \tag{10.43}$$

while the random walk of the reptation tube is

$$< |\vec{r}(t) - \vec{r}(0)|^2 > \approx r_t \sqrt{< |s_j(t) - s_j(0)|^2 >} \approx r_t^2 \left(\frac{N}{N_e}\right)^{1/2} \left(\frac{t}{\tau_R}\right)^{1/2}. \tag{10.44}$$

And finally at $t > \tau_{rep}$ the chain motion averages over all tubes and Fickian diffusion has to be recovered $< |\vec{r}(t) - \vec{r}(t)|^2 >= 6 D_{rep} t$ where $D_{rep} \approx \frac{R_0^2}{\tau_{rep}} \approx \frac{k_B T}{\beta} \frac{N_e}{N^2}$.

The four regimes can be summarized into a plot that shows the regimes with the marked relaxation times, Figure 10.14. indicating the sub-diffusive motion at

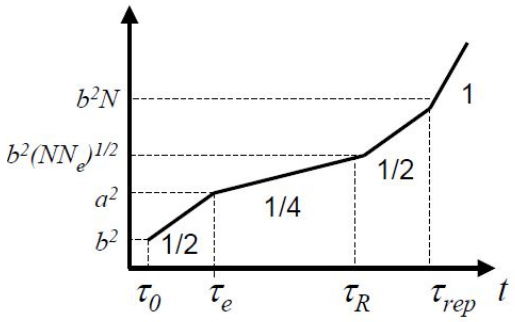

Figure 10.14: Diffusivity of entangled polymers as a function of time. At long time scales ($t > \tau_R$) the coil behaves like a particle and the mean square displacement increases linearly in t. At smaller times the monomer times and the entanglement slow down the dynamics considerably indicated by the slower scaling with t at smaller times.

small time scales while the scaling with t^1 is recovered for long times. At these long time scales polymers behave as simple liquids while at the shorter time scales dynamics are slowed down due to entanglement, and finally on the monomers the connectivity of the segments described by Rouse and Zimm determines the polymer dynamics.

Reptation and gel electrophoresis

Charged polymers diffuse through a gel due to applied potential. The reptation picture describes polymer motion very well if the field strength is low and the polyelectrolyte is longer than the typical pore size of the gel. DNA moves in the direction of the applied field as expected as large-scale EOF is suppressed by the low charge of the gel fibres and the hydrodynamic resistance.

In contrast to the free solution electrophoresis we expect a $1/L$ dependence of mobility as well as a dependence on the pore size of the gel. This is experimentally observed as can be seen in Figure 10.15. In general this holds for DNA molecules

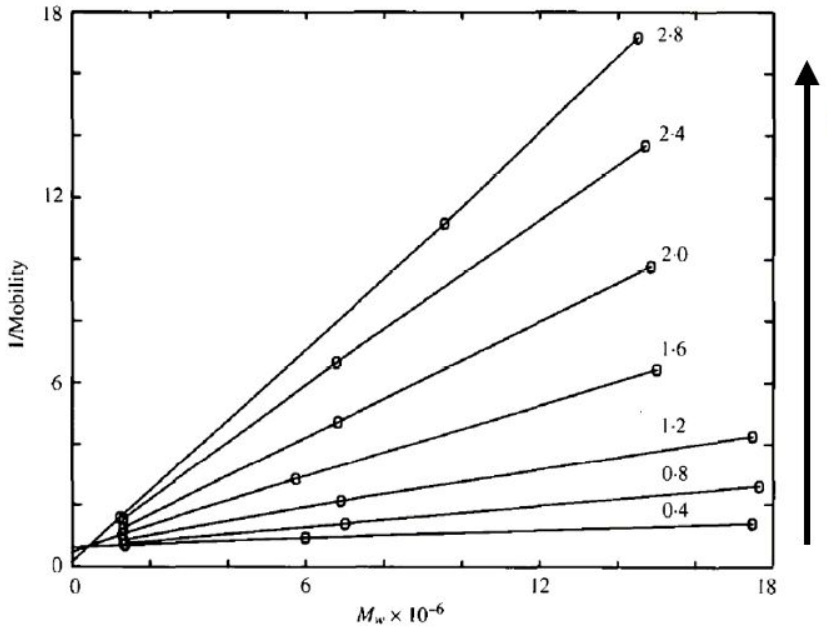

Figure 10.15: Plot of reciprocal of mobility in arbitrary units against molecular weight (length) of DNA molecules in gels. Numbers on lines are concentrations of agarose in percent, higher density denotes smaller pore size and smaller mobility. 1/Mobility scales linearly with $1/L$ and separation by molecular size is possible despite the identical ζ-potential of the molecules.

that are much longer than the Debye screening length. As already mentioned the chains should be longer than the typical pore diameter in the gel.[2] The range of DNA length for a typical agarose gel with 1% density is shown in Figure 10.16 for DNA of 200bp to 20,000bp in molecular weight. Since for very short DNA the mobility is almost the same for all length the polyelectrolytes have to be separated

[2]For very long polymers the model breaks down as trapping and knots become more frequent and long time trapping is very important.

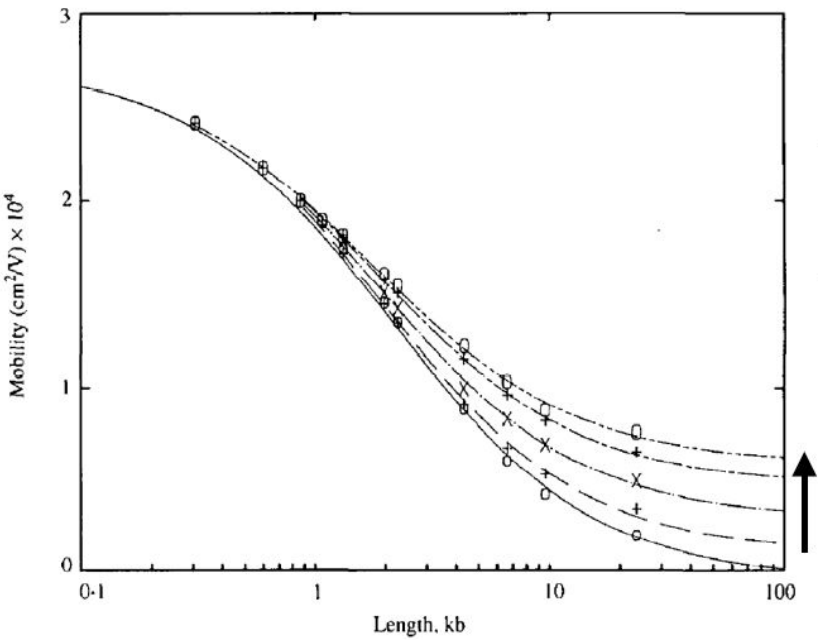

Figure 10.16: Electrophoretic mobility of double-stranded DNA in 1 percent agarose gel as a function of DNA length and for different electric fields. Electric field is increasing as indicated by the arrow.

over long timescales. For separation of DNA with a length of more than 40 kilobasepairs in length there are better methods like pulsed field gel electrophoresis.[3].

10.5.3 Tether force in electrophoresis

We focus on one aspect of electrophoresis, the so-called tether force. The thether force is needed to hold a charged object in place against the action of an externally applied electric field. This situation corresponds to a DNA molecule that is temporarily trapped in a metastable configuration inside a gel. The movement is stalled as the DNA molecule is wrapped around a gel fibre or a knot has formed that prevents further movement.

In order to focus on the key concepts, we reintroduce the system of two parallel plates as earlier in this chapter (see Figure 9.7). The system consists of a charged surface with a uniform surface charge density s separated from a second, parallel surface that is electrically neutral. For most systems of interest, σ has a negative value; while this is not assumed in our derivation, the plots in the figures correspond to this case. The charged surface has a surface area A, and the

[3]There are also intensive efforts to replace these gels with artificial 'gels' made by semiconductor nanotechnology or single molecule methods based on nanopore based single-molecule sensing

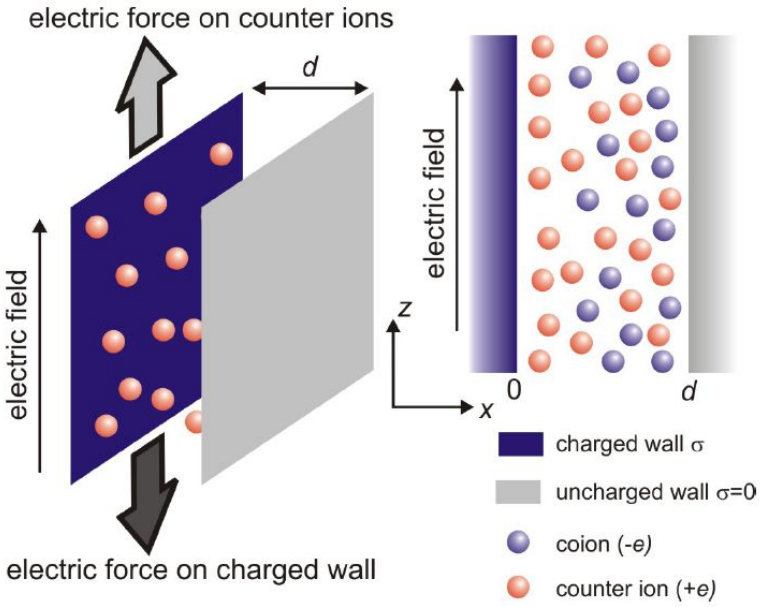

Figure 10.17: A negatively charged surface (left) is immersed in an ionic solution and located a distance d from a second, uncharged surface (right). A uniform electric field acts on the charged wall and the ions in solution. An electric field is applied and to the system along the z-direction and the force on the left plate can be measured.

surfaces are separated by a distance d. We assume that the lateral dimensions of the charged surface are sufficiently large that edge effects can be neglected; under these conditions all of the relevant equations become one-dimensional. The volume between the two planes is filled with an electrolyte, which is in diffusive equilibrium with a bulk reservoir. We take the electrolyte as consisting of water containing a number density n_0 of a fully dissociated monovalent salt. A good example of the latter is potassium chloride (KCl), which dissociates into K^+ and Cl^- ions in water. This implies that in bulk solution there is a number density n_0 of both positive ions (also known as cations) with charge $+e$ and negative ions (anions) with charge $-e$, where e is the charge of the electron. We treat water as a homogeneous medium with permittivity $\epsilon_w = 80\epsilon_0$. A uniform electric field with magnitude E is applied parallel to the surface and permeates the region between the surfaces. The direction of this electric field is defined as z, while the direction perpendicular to the planes is x (with $x = 0$ corresponding to the position of the charged surface and $x = d$ to that of the neutral surface). We will further assume that σ is small and that d is large, as defined more quantitatively below.

We derived the ion distribution in the double layer within the so-called PoissonBoltzmann formalism. At equilibrium, the average concentration of charged molecules at position x is assumed to follow the Boltzmann distribution. We also

discussed the EOF that is resulting in the gap and its dependence on the plate distance.

We will now use the EOF velocity to calculate the tether force F_{mech} that must be applied to hold the charged surface in place against the action of the electric field. The relevant forces are summarised in Figure 10.18. In the following the superscripts σ and 0 refer to the charged and uncharged surfaces, respectively.

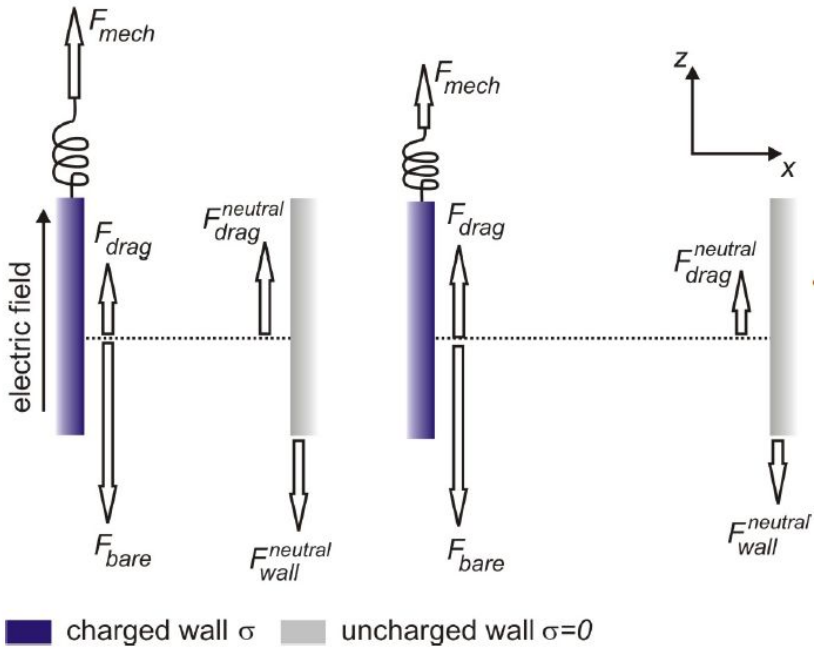

Figure 10.18: Force balance. (a) The electric field pulls the negatively charged wall towards the bottom of the image with force F^{σ}_{bare}. The counterions (not shown) experience a force in the opposite direction. This leads to drag forces F^{σ}_{drag}, acting on the charged surface, and F^{0}_{drag}, acting on the uncharged surface. To hold the system in place, a tether force F^{σ}_{mech} (represented by a spring) must be applied to the charged wall, and an equal but opposite force F^{0}_{mech} must be applied to the uncharged wall. (b) When the distance d is increased, the drag force on the charged wall increases. Correspondingly, the drag force on the uncharged wall F^{σ}_{drag} and the tether force F^{0}_{mech} decrease. This is a direct result of the higher flow velocity of the liquid through the larger gap between the walls.

The total force applied to the charged surface by the electric field can be decomposed into two components that always act simultaneously. First, the electric field acts directly on the charges of the surface. We refer to this component as the bare force, F^{σ}_{bare}, since this is the force that would be experienced by the bare surface if it was suspended in vacuum. This force follows simply from Coulombs law and is given by $F^{\sigma}_{bare} = A\sigma E$. The electric field simultaneously acts on the oppositely charged screening cloud and sets up an electroosmotic flow, as discussed

in the previous paragraphs. Because this flow causes the fluid to be sheared at the boundary with the charged surface, it exerts a drag force F^{σ}_{drag} on the charged surface whose value is given by Newtons relation as

$$F^{\sigma}_{drag} = a\eta \left| \frac{dv_{eof}(x)}{dx} \right|_{x=0} = -ae\sigma \left(1 - \frac{\lambda}{d}\right) = -\left(1 - \frac{\lambda}{d}\right) F^{\sigma}_{bare}. \quad (10.45)$$

The mechanical tether force follows directly from the above and is given by

$$F^{\sigma}_{mech} = -F^{\sigma}_{elec} = -(F^{\sigma}_{bare} + F^{\sigma}_{drag}) = -AE\sigma\frac{\lambda}{d}. \quad (10.46)$$

This result contrasts strongly with what would be expected in the absence of the drag force induced by the screening charge: in that case we would expect $F^{\sigma}_{bare} = -AE\sigma$, which is larger than the correct answer by a large factor, d/λ.

The calculation thus indicates that drag from the counterions, far from being a minor correction, is in fact a dominant factor in determining the magnitude of electrophoretic forces. Furthermore, its influence does not depend solely on local properties in the vicinity of the charged surface, but instead encompasses all aspects of the environment that modify the electroosmotic flow, its magnitude and distribution. This is made explicit by the appearance of d in our equation for F^{σ}_{mech}. It is also manifest in the distribution of ions and potential $\phi(x)$ which are essentially independent of d (so long as $d \gg \lambda$). However the flow profile shown in Figure 10.4 is strongly affected by the value of d.

Further insight can be gained by considering the uncharged wall. Although the electric field does not act directly on this wall, the electroosmotic flow does exert a drag force on it since the shear stress is non-vanishing at $x = d$. Following the same steps as above we have for this force

$$F^{0}_{mech} = -A\eta \left| \frac{dv_{eof}(x)}{dx} \right|_{x=0} = AE\sigma\frac{\lambda}{d} = -f^{\sigma}_{mech}. \quad (10.47)$$

The forces on the two walls are thus equal and opposite, which may at first appear surprising. It is however easily understood by considering that the electric field exerts no net force on the system as a whole since the force exerted on the charged wall is exactly compensated by the force on its screening charge. Any external mechanical force on the charged wall must therefore be balanced by a second external force. Equivalently, one can consider that the total force on the screening charge is transmitted to the two surfaces through shear in the fluid. The fraction that reaches the uncharged surface is λ/d, while the fraction that reaches the charged surface is $(1 - \lambda/d)$. It follows directly that $F^{\sigma}_{mech} = -(F^{\sigma}_{bare} + F^{\sigma}_{drag}) = -F^{0}_{mech}$.

Our result predicts that the tether force F^{σ}_{mech} goes to zero as the distance d is increased toward infinity, and therefore that there is no tether force on a charged

surface far from any boundary. This counterintuitive result is actually an artefact caused by the approximations that we have made. In particular, we have neglected edge effects and essentially treated the charged surface as infinite. For a finite-sized surface, a small but non-zero force remains due to a back flow of fluid on the size scale of the surface itself. More generally, we have neglected inertial effects by using only the Stokes equation to describe the motion of the fluid. On large enough length scales, however, inertia becomes relevant as the Reynolds number increases and our approximation breaks down.

In simple electrostatics, the force on a charged object is proportional to its charge multiplied by the local electric field. As we saw in the previous section, on the other hand, the net tether force on a charged object in an electrolyte is not simply given by its bare surface charge density, and is instead much smaller due to an important contribution from the screening layer. To an observer who is unaware of what is happening in solution and who simply measures the tether force in response to a known electric field, however, it is natural to describe the force as resulting from an effective surface charge density σ_{eff}, such that $F^{\sigma}_{mech} = -A\sigma_{eff}E$, with $|\sigma_{eff}| < |\sigma|$. σ_{seff} is thus also defined by the geometry of the experiment and $\sigma_{eff} = \sigma(\lambda/d)$.

The effective charge, as introduced above, is a well-defined quantity, both experimentally and theoretically. Nevertheless, the use of the concept of effective charge should be always associated with the following important limitations. First, the effective charge does not correspond to a physical charge, but rather includes factors that depend on the geometry of the hydrodynamic environment around the charged object. Second, because the effective charge is not an intrinsic property of the charged object, instead depending on geometry parameters such as d, its value cannot be compared directly between different experimental configurations. Comparisons between tether force and electrophoretic mobility experiments are even more difficult, as the relation between the effective charges that are commonly defined in these two experimental situations is model-dependent. Third, the concept of effective charge is ineffective as a pedagogical tool as many readers are left with a vague notion that the effective charge consists of the bare charge of the object, minus some countercharge which is physically immobilized on the object. While this sort of complexation can certainly be an important contribution in real systems, thinking about electrophoresis solely in this manner obscures the fact that the tether force is expected to be smaller than the bare value even if there are *no* immobile countercharges.

10.5.4 Force on a polymer in cylindrical confinement

This section uses the physical principles discussed above and shows an example for the use of Bessel functions outside optics.

In describing the ionic screening of charged, stiff biopolymers such as DNA, a common approximation is to treat the molecule as a charged, solid cylinder. Analogous to the discussion of the infinite plane above, we focus here on a charged cylinder with radius a and surface charge density σ positioned in the center of a larger, uncharged cylindrical cavity with radius R. For such a problem with cylindrical symmetry, the PB equation takes the form

$$\frac{1}{r}\frac{d}{dr}\left(r\frac{d\phi(x)}{dr}\right) = \frac{2en_0}{\epsilon_w}\sinh\left(\frac{e\phi(r)}{k_BT}\right) \approx \frac{\phi(r)}{\lambda^2} \tag{10.48}$$

where the last step corresponds to the DebyeHückel approximation. In this last case and for $R \ll \lambda$, the corresponding solution for the potential is

$$\phi(x) = \frac{\sigma\lambda}{\epsilon_w}\frac{K_0(r/\lambda)}{K_1(R/\lambda)} \tag{10.49}$$

where K_0 and K_1 are the 0th and first order modified Bessel functions of the second kind, respectively. Analogous to the planar geometry, the potential decays exponentially away from the charged cylinder.

For a highly-charged surface, the linearization is no longer valid and the full PB equation must be solved. We only note that the resulting solution exhibits the same qualitative features as for the case of a plane, and once again the screening charge can be broken into a diffuse layer, whose size is given by the Debye length, and a compact layer, characterized by the GouyChapman length. The amount of charge in the diffuse layer also saturates at a constant value with increasing σ, while the remaining screening charge resides in the compact layer and consists primarily of counterions.

This separation into two components can be made more precisely in the special case of a line charge (a cylinder with $R \to 0$) with linear charge density ρ and in the absence of supporting salt ($n_0 = 0$). In this case ions accumulate (or condense) on the line charge, partly compensating its charge until its value decreases to a magnitude e/l_B where $l_B = e^2/4\pi k_BT\epsilon_w$ is the Bjerrum length. The linear charge density of the condensed ions is thus ($|\rho| - e/l_B$), while the linear density of charge in the diffuse layer is the remaining e/l_B. This result, known as Manning condensation, often serves as a first approximation for the composition of the double layer in more realistic cases. Double-stranded DNA, for example, has a charge density of $2e$ per base pair, corresponding to $\rho = 4.2e/l_B$. This is well over the critical threshold for counterion condensation to occur, and as a first estimate a fraction $1 - \frac{1}{4.2} = 0.76$ of the charge can be expected to be screened by condensed counterions.

The force balances and the corresponding EOF velocity in the cylindrical geometry are shown in Figure 10.19. Because the distribution of screening charge

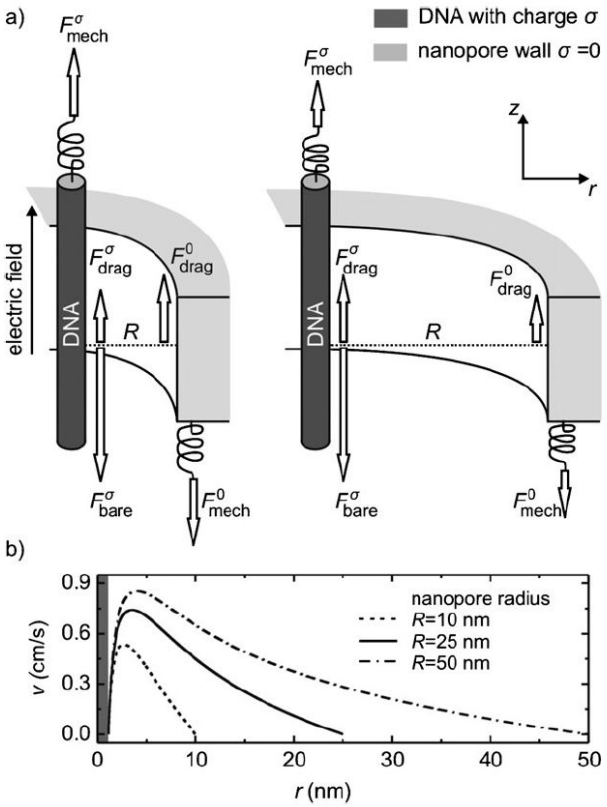

Figure 10.19: Force balance for DNA in the center of cylindrical confinement with radius R. (a) Left: the balance of forces is qualitatively identical to the case of planar surfaces. The DNA is stalled by a tether force F^{σ}_{mech} applied to the DNA, while an equal but opposite force F^{0}_{mech} acts on the uncharged wall. Right: for increased radius R, the drag force on the DNA also increases. Correspondingly, the drag force on the wall F^{0}_{drag} and the tether force F^{σ}_{mech} decrease. (b) The flow velocity $v(r)$, calculated by numerically solving the full PB equation and combining the result with the Stokes equation. The maximum flow velocity depends on the radius R, as in the case for parallel plates but the shape if different.

in the vicinity of a charged cylinder is qualitatively very similar to that near a surface, our discussion of electroosmotic flows and tether forces applies directly to the case of a cylinder. In particular, as illustrated above, here also the tether force is due to a combination of bare electrostatic force and a drag force from the counterions, with the drag force being of comparable magnitude to the bare force. The cylindrical geometry only influences our analysis and conclusions at a quantitative level. For example, the figure above shows the fluid velocity $v(r)$ as a function of radial position r. Far from the charged cylinder, $v(r)$ exhibits a non-linear decay with increasing r, unlike our result for planar surfaces, leading to subtle differences in how the drag force is distributed between the two surfaces. However, this does not fundamentally change the interpretation of the tether force.

The tether force is directly experimentally accessible by measuring the force on single DNA molecules in gels or small channels with the help of optical tweezers.

Chapter 11

SCM Problems part II

These are the questions on the second part of the Part II soft condensed matter course by Keyser and Knowles.

Lent and Easter Terms 2021

Version: January 9, 2023

II-Q 1 The concentration of aqueous solutions of butanol, and their surface tension with air were measured at 20^{o}C with the following results:

c/mol dm^{-3}	0.0264	0.0536	0.1050	0.2110	0.4300
γ/ mN/m	68.00	63.14	56.31	48.08	38.87

Determine the surface area available per molecule of butanol.

II-Q 2

(a) The amphiphilic molecule sodium dodecyl sulphate (SDS) has the following dimensions: length of hydrophobic tail $l_c = 1.67$ nm, volume of hydrophobic tail $v = 0.35\,\text{nm}^3$, area per head group $a = 0.57\,\text{nm}^2$. Assuming that SDS forms spherical micelles, calculate the micelle radius and the mean aggregation number. What does your result suggest for the formation of micelles of SDS? Briefly discuss your conclusion.

(b) Show that for a lipid bilayer made by surfactant molecules with effective tail length l, volume v and head group area a:

$$\frac{1}{2} < \frac{v}{al} < 1.$$

II-Q 3 Ignoring any effect from gravity, the amplitude spectrum of thermal fluctuations of the interface between two fluids, as a function of the wavevector **q**, is approximately:

$$\langle h^2(\mathbf{q})\rangle = \frac{k_B T}{A(\gamma q^2)}.$$

where γ is the interface tension and A is the area of the interface. This interface is in a square container with $A = 1\,\mathrm{cm}^2$.

At room temperature, what is the average undulation amplitude due to thermal fluctuations for the interface between water and hexane, which has an interface tension of 38×10^{-3} N/m?

[*Hint: Assume a small wavelength cutoff at the molecular scale of 0.2 nm.*]

II-Q 4

(a) At room temperature, water wets a clean glass surface almost completely. Water is observed to rise to a height of 4.7 cm in a capillary tube of 0.8 mm diameter. Calculate the surface tension of water.

(b) Liquid of viscosity η is taken up by a capillary of radius R at a rate given by the Poiseuille equation. If the contact angle for the liquid on the capillary surface is θ, and the surface energy is γ, show that the distance, L, the liquid has traveled up the capillary in time t is given by:

$$L(t) = \sqrt{\frac{R\gamma\cos(\theta)t}{2\eta}}.$$

II-Q 5 Calculate the variation of energy δW needed to move the contact line between a solid, vapour and a partially wetting liquid. You may assume that the system is in equilibrium. Your answer should yield Young's equation.
Now use the wetting parameter S as defined in the lectures to derive a relationship between S and $\cos\theta$ to relate contact angle to surface tension and S.

II-Q 6

(a) Explain how a surfactant can be used to stabilise an emulsion between water and oil. You may use a sketch.

(b) A water-in-oil emulsion is stabilised by a surfactant. The surfactant is only present in the aqueous phase at concentration c_0 (by volume). The surfactant

concentration in the oil phase is $c = 0$. Now an emulsion of water in oil is formed. The concentration of surfactant on the droplet surface is given by c_S while its concentration in the aqueous droplet is c_v. Find an equation that connects the starting (bulk) concentration c_0 with the surfactant concentration c_s (droplet surface) and c_v (droplet volume). How does c_s scale with the droplet size?

(c) Discuss the challenges for stabilising shrinking droplets given your result from part (b)?

II-Q 7 Assuming that the interatomic potential between two atoms a distance r apart is given by $-L/r^6$, show that the attractive potential per unit area between two semi-infinite plates (i.e. blocks facing each other, semi-infinitely deep and infinitely wide and high) a distance h apart is given by $-A/(12\pi h^2)$, where the Hamaker constant A is given by $\pi^2 n^2 L$ and n is the number of atoms per unit volume.

II-Q 8 In the Debye-Hückel approximation the Poisson-Boltzmann equation for the potential of charges in electrolyte near a surface is solved by linearisation.

(a) Obtain the variation of the potential as a function of distance from the surface and discuss the role of the Debye-Hückel approximation.

(b) What is the physical meaning of the Debye screening length?

(c) How does the Debye screening length and the validity of the Debye-Hückel approximation change if salt is added to the solution?

II-Q 9 Solve the Poisson-Boltzmann equation (Eq. (5.6) in the notes) for the spherically symmetric situation:

$$\frac{1}{r^2}\frac{d}{dr}\left(r^2\frac{d\psi}{dr}\right) = \frac{e^2\beta\psi(r)}{\epsilon}\sum_i c_{0,i}z_i^2 \tag{11.1}$$

II-Q 10

(a) Ions are not point-like and have a finite radius a. The Debye-Hückel theory can be expanded to include finite ion size. Assume that ions are hard spheres with radius a and charge q. For simplification the dielectric constant of ion and solvent are the same. Calculate the potential around the ion for $r > a$ and $0 < r < a$.

(b) Calculate the charge distribution around and sketch the distribution as a function of distance. Determine the maximum of the distribution.

II-Q 11 A charged particle with radius R and charge Q is immersed in aqueous solution containing monovalent ions. Assume that the ions have a radius a_i. You may start from the Debye-Hückel potential around the particle

$$\phi(r) = \frac{Q}{4\pi\epsilon_0\epsilon}\frac{\exp(-\kappa(r-a))}{r(1+\kappa a)}\,, r > a$$

where $a = R + a_i$ the effective radius of the spherical particle. κ is the inverse of the Debye screening length. Determine the surface potential of the particle at $r = R$ and interpret your result.

II-Q 12 The electric double layer (EDL) can be seen as a capacitor.

(a) Calculate the capacitance of the EDL in concentrated electrolytes for an electrode with area of 1 cm^2 in water ($\epsilon = 80$) when the radius of a hydrated ion is 0.2 nm. In experiments the capacitance is found to be 10 μF. Explain the discrepancy between your result and the experimental result.

(b) Calculate the electric field strength in the system given in (a) when the surface potential is 100 mV.

(c) What happens with the capacitance in dilute electrolyte solutions?
[*Hint: Consider the full structure of the double layer and what determines the capacitance.*]

II-Q 13

(a) Consider charged spherical colloid particles of radius a, with their surface carrying a charge σ per unit area, in an ionic solution with the equilibrium ion concentration is n_0. Find the electrostatic potential at the surface of a colloidal particle ψ_0.

(b) To obtain the interaction between two charged colloid particles, you should consider the electrostatic repulsion between them, and the osmotic pressure at the mid-point plane between them. Compare the two effects for the case of two spherical particles at significant separation, and also for the case of two planar (half-space) parallel surfaces a distance h apart.

(c) Sketch the combined interaction energy between two colloidal particles as a function of their separation (DLVO). Explain the relative energy scales of the contributions to interaction. Describe an experiment whereby the force of this interaction can be measured.

II-Q 14

(a) Electrophoresis is a process frequently used to separate proteins of slightly differing charge or size, dispersed in water. Obtain an expression for the drift velocity for capillary electrophoresis, modeling the protein as a sphere of radius R and charge Ze.

The mutant and native forms of a protein, both with radius 3nm, differ in charge by e. If an electric field of $500\,\mathrm{Vm}^{-1}$ is applied, and the minimum separation of the two bands produced by the two species which can readily be detected is 1mm, how long will the electrophoresis experiment need to be carried out to differentiate the two species?

[Take $\eta_{water} = 1 \times 10^{-3}$ Pa s at room temperature.]

(b) If we take diffusion into account, what is the broadening of the bands at the end of the experiment?

II-Q 15 Assume that the surface of a cylindrical capillary of radius r is charged and has a fixed surface potential $\phi_0 < 0$. Under the assumption that $r \gg \lambda$ show that the fluid velocity v of the electro-osmotic flow in the centre of the capillary can be written as

$$v = -\frac{\epsilon_0 \epsilon_r \phi_0 E}{\eta}$$

where η is the fluid viscosity and E the applied electric field along the capillary. Explain why this velocity does not depend on r.

[*Hint: You may assume low Reynolds number i.e. laminar flow conditions. Boundary conditions on the capillary surface are no-slip, which means velocity* $v = 0$ *at* $x = 0$*. This calculation is done in the thin Debye layer limit which means* $\partial v/\partial x = 0$ *for distances from the surface larger than the Debye length. You will need to combine the Poisson equation linking surface potential and charge density*

$$\frac{\partial^2 \phi}{\partial x^2} = -\frac{\rho(x)}{\epsilon_r \epsilon_0}$$

with the Stokes equation

$$-\eta \frac{\partial^2 v}{\partial x^2} = \rho(x) E$$

and solve the resulting differential equation by integration and taking the boundary conditions into account.]

II-Q 16 Consider a spherical particle in water with radius $r = 2$ μm held in an optical trap far from any surface. The charged particle is in an homogeneous electric field $E = 10$ V m^{-1} in aqueous solution with the viscosity of water $\eta = 0.001$ kg m^{-1}s^{-1}.

(a) Assuming a surface potential $\phi = -20$ mV calculate the expected electrophoretic force F_e and displacement from the centre of the optical trap Δx. You may assume that the optical trap forms a harmonic potential with linear force distance relation $F = -\kappa\Delta x$ where $\kappa = 0.1$ pN nm^{-1}. What is the maximum velocity of the counter ions in the EDL around the particle at $E = 10$ V m^{-1}?

(b) Sketch the forces acting on the particle in (a).

(c) A particle in an optical trap undergoes Brownian motion. The variance of the fluctuations $\langle x^2 \rangle$ are linked to the stiffness κ of the optical trap by the equipartition theorem. In a real experiment, $\langle x^2 \rangle$ is found to be 4.14×10^{-17} m^2 at $E = 0$ and 3.52×10^{-17} m^{2}at $E = 10$ V m^{-1}. Estimate the stiffness of the optical trap. Is the trap harmonic?

[*Hint:* $\gamma = 6\pi\eta r$ *is the Stokes friction coefficient of the particle.*]

II-Q 17 A flexible polymer with N Kuhn segments of length b is moving inside a gel. The gel fibers are spaced far enough apart to only marginally affect the conformation of the polymer chain.[1]

(a) Assume that the polymer has a drag coefficient of $\gamma = \eta N b$ in the gel, with η the viscosity of water and b the segment length. Find an expression for the time, τ, it takes for the polymer to diffuse a distance equal to its contour length $L = Nb$. Using this expression, estimate τ for double-stranded DNA ($b = 100$ nm) with a length of 30,000 basepairs.

(b) An uniform electric field E is applied in the gel which leads to a total force $F = fN$ on the polymer. Assume that the polymer moves through the gel by reptation only and hence show that the drift velocity v_d of the polymer in the gel is now depending on N

$$v_d = \frac{f}{\eta b N}.$$

[1]Part of this question is based on Zimm and Levene, "Problems and prospects in the theory of gel electrophoresis of DNA" Quart. Rev. Biophys (1992). Can be downloaded from the course webpage.

(c) Estimate the electric field E that you need to drive DNA molecules with 30,000 basepairs through a gel of 10 cm length in 1 hour. Calculate the distance DNA molecules with 25,000 basepairs would have traveled in the same amount of time. In both cases you may assume that the DNA has a charge of $600e$ per 100 nm segment.